



FACILITY FORM 002	N67 13192	(ACCESSION NUMBER)		(THRU)
	<del>13192</del> 87	(PAGES)		1
	CR - 66206	(NASA CR OR TMX OR AD NUMBER)		06
				(CATEGORY)

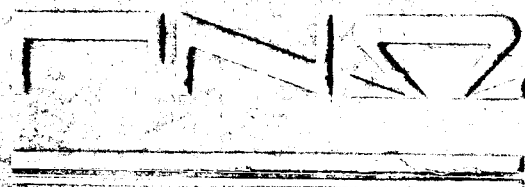
GPO PRICE \$ \_\_\_\_\_

CFSTI PRICE(S) \$ \_\_\_\_\_

Hard Copy (HC) 2.50

Microfiche (MF) .75

ff 853 July 65



**FRANKLIN GNO CORPORATION**

P.O. BOX 3250 WEST PALM BEACH FLORIDA 33402

A FUNDAMENTAL STUDY OF ELECTROPHILIC GASES  
FOR PLASMA QUENCHING

BY

Robert W. Crowe  
and  
W. D. Kilpatrick

Distribution of this report is provided in the Interest of Information Exchange. Responsibility for the contents resides in the author or organization that prepared it.

Prepared under Contract No. NAS1-5575

By: Franklin GNO Corporation  
P. O. Box 3250  
West Palm Beach, Florida

For:  
National Aeronautics and Space Administration  
Langley Research Center

## FOREWORD

The research reported herein has been directed toward obtaining basic scientific information to be used for the quenching of plasmas created during re-entry flight. The study is both an experimental and theoretical one of electron attachment by certain chosen materials.

This research was sponsored by the Langley Research Center, National Aeronautics and Space Administration under Contract NAS1-5575, and covers work completed between October 15, 1965, and October 15, 1966.

The authors wish to recognize the special contributions of Mr. Robert C. Kindel in carrying out the experiments performed during the contract period.

ABSTRACT

The electron attachment properties of several high molecular weight gases were examined:  $C_6F_{14}$ ,  $C_7F_{16}$ ,  $C_8F_{18}$ ,  $C_8F_{16}O$ , Freon E-3, Freon E-4, Freon E-5, and  $SF_6$ . Simplified calculations for quiescent plasma quenching have been made based on data from room temperature measurements.

One measurement technique employed negative ions of these gases in a drift tube such that negative ion mobility could be measured. The mobilities of the negative ions for the gases in air at concentrations of 10 to 0.5% gave results essentially in agreement with Blanc's law for concentrations, but electron attachment was complete for all samples, independent of concentration.

A second measurement technique of high voltage breakdown was used for investigating high temperature decomposition of  $C_7F_{16}$ ,  $C_8F_{18}$ ,  $C_8F_{16}O$ , and  $SF_6$ . In addition to determining high voltage breakdown coefficients for the gases, it was determined that 700 - 800° K represents an approximate threshold for decomposition. Daughter compounds were also electrophilic.

AUTHOR

TABLE OF CONTENTS

	FOREWORD	i
	ABSTRACT	ii
	LIST OF ILLUSTRATIONS & TABLES	v
SECTION I	INTRODUCTION	1-1
SECTION II	ELECTRON ATTACHMENT BY ELECTROPHILIC GASES	2-1
	2-1 Properties of Chosen Electrophilic Materials	2-1
	2-2 Experimental Procedure for Electron Capture Measurements	2-1
	2-2-1 The Vacuum System	2-1
	2-2-2 The Drift Chamber	2-2
	2-2-3 The Principle of Operation	2-2
	2-2-4 Calibration of Equipment	2-6
	2-2-5 Calculations of Ion Pulse Dimensions	2-7
	2-2-5-1 Case I; $t_1 \ll t, t_1 \ll 1/Z_a$	2-9
	2-2-5-2 Case II; $t_1 \cong t \cong 1/Z_a$	2-10
	2-3 Experimental Observations of Electron Attachment	2-12
	2-3-1 Method for Analyzing Data of Electron Capture	2-12
	2-3-2 Typical Recorder Tracings	2-12
	2-3-3 Significance of Ion Peaks	2-13
	2-3-3-1 Ion Mobility	2-13
	2-3-3-2 The Photopulse	2-14
	2-3-3-3 The Meaning of $Q/Q_0$	2-15
	2-3-3-4 Typical Calculations	2-16
	2-3-4 Experimental Results Obtained	2-16
	2-3-4-1 Additional Improvements Made in Electronic Components	2-16

TABLE OF CONTENTS (cont.)

	2-3-4-2 Experimental Observations for Typical Electrophilic Materials in Air	2-17
	2-3-4-3 Tabulation of Attachment Results	2-18
	2-4 Discussion and Analysis of Attachment Data	2-18
	2-4-1 Observed Values of $Q/Q_0$	2-18
	2-4-2 Direct Measurement of Attachment Coefficient	2-18
SECTION III	HIGH VOLTAGE BREAKDOWN OF ELECTROPHILIC GASES AT ELEVATED TEMPERATURES	3-1
	3-1 Technical Background	3-1
	3-2 Details of High Voltage Breakdown	3-2
	3-2-1 Avalanche and Breakdown	3-2
	3-2-2 High Temperature Breakdown	3-3
	3-2-3 Thermal Stability of the Perfluorocarbons	3-5
	3-3 Results of Experimental Breakdown	3-5
	3-3-1 Apparatus	3-5
	3-3-2 Sulfur Hexafluoride ( $SF_6$ )	3-6
	3-3-3 Perfluoroheptane ( $C_7F_{16}$ )	3-7
	3-3-4 Perfluorooctane ( $C_8F_{18}$ )	3-7
	3-3-5 Cyclic Perfluoroether (c- $C_8F_{16}O$ )	3-8
	3-4 Discussion of Breakdown Data	3-8
SECTION IV	CALCULATION OF EQUILIBRIUM QUENCHING	4-1
SECTION V	SUMMARY & CONCLUSIONS	5-1
REFERENCES		

LIST OF ILLUSTRATIONS

Figure		Following Page
1	Vapor Pressure Data for Several Chosen Materials	2-1
2	Schematic Block Diagram, Vacuum System	2-2
3	Schematic Diagram of Drift Chamber	2-2
4	Pulsing Sequence for Attachment Measurements	2-4
5	Block Diagram of the Experimental System	2-4
6	(A) Typical Grid Bias Pulsing Sequence (B) Cathode Pulsing Sequence with Positive Grid Pulse Showing	2-5 2-5
7	(A) Cathode and Photo Pulsing Sequences Measured Simultaneously (B) Expanded Oscillogram of Above Sequences ...	2-6 2-6
8	Recorder Tracings	2-7
9	Calculated Electron Density $x = )$ and Different Pulse Length, $Z_a = 10^4/\text{sec}$ .	2-10
10	Calculated Electron Density Distribution for Continuous Emission, $Z_a = 10^4/\text{sec}$ .	2-11
11	Recorder Tracings	2-16
12	Time Distribution of all Ionic Charges per Second Arriving at the Control Grid for one Photopulse	2-16
13	Recorder Tracings	2-18
14	Recorder Tracings	2-18
15	Log I vs t for $O_2$ at $E/P = 0.25 \text{ volt/Torr cm}$	2-19
16	Log I vs t for Freon E-3 Diluted in Air	2-20

LIST OF ILLUSTRATIONS (cont.)

Figure		Following Page
17	Typical Prebreakdown Avalanche Currents	3-3
18	Comparison of Thermal Stabilities Shown by Heat of Formation from Atoms	3-5
19	High Voltage Breakdown Apparatus, Schematic	3-5
20	Dimensions in Inches of Quartz Test Cell & Electrodes	3-6
21	Voltage Breakdown Characteristic for SF <sub>6</sub> vs T, P	3-6
22	Voltage Breakdown vs T, P for Sulfur Hexafluoride	3-6
23	Breakdown Voltage for Perfluoroheptane as a Function of Pressure and Temperature	3-7
24	Voltage Breakdown vs T, P for Perfluoroheptane	3-7
25	Voltage Breakdown Characteristic for (C <sub>8</sub> F <sub>18</sub> ) as a Function of Temperature and Pressure	3-7
26	Voltage Breakdown vs T, P for Perfluorooctane	3-7
27	Voltage Breakdown Characteristic for (C <sub>8</sub> F <sub>16</sub> O) as a Function of Temperature & Pressure	3-8
28	Voltage Breakdown vs T, P for Cyclic Ether	3-8
29	Voltage Breakdown Constants at Room Temperature vs Molecular Weight for Fluorocarbons	3-8
30	Data for Breakdown at Room Temperature for Gap of .193 cm	3-8
31	Temperature Variation of Electrophilic Breakdown with Constant P δ	3-8
32	$\beta t$ vs $\rho_e$ for Various Values of $(\rho_M)_0$	4-3
33	$\beta t$ vs $(\rho_M)_0$ for Specific Values of $\rho_e$	4-3



LIST OF TABLES

			On Or Following Page
Table	I	Results of Mobility Measurements of $SF_6^-$ in $SF_6$	2-6
	II	Attachment Data for Mixtures of Perfluorocarbons in Air	2-18
	III	Breakdown Constants for the Relation $V_s \sim k_1 P\delta + k_2$	3-9

## SECTION I

### INTRODUCTION

It has been realized for a number of years that free electrons are produced in the upper atmosphere from various causes. Natural processes, involving radiation from the sun, produce these electrons by photoionization and photodetachment. They are also produced by the passage of meteors through the upper atmosphere.

In addition to the above, there are a number of "man-made" phenomena which result in the production of large quantities of free electrons in the upper atmosphere. Among these are the various ionization mechanisms following atmospheric nuclear explosions, thermal processes in the exhausts of rockets, and thermal ionization caused by space vehicles as they re-enter the earth's atmosphere. In the latter case, the free electrons produced act as reflectors of electromagnetic radiation if present at sufficiently high density. Consequently, they are responsible for the communications "black-out" which is sometimes associated with vehicle re-entry. The extent of this black-out is, of course, strongly dependent upon the concentration of free electrons in the vicinity of the antenna of the re-entry vehicle.

Among the methods being used in an effort to eliminate communications black-out are attempts to reduce the electron concentration by what is known as plasma quenching. It is often necessary to decrease the density of electrons by from 3 to 4 orders of magnitude to accomplish this. Plasma quenching is essentially a process which alters the characteristics of the plasma. In general, such alterations result in a reduction in electron concentration.

From about the beginning of the 20th century, many experiments have been conducted in an effort to determine the behavior of charge carriers in a gaseous medium. Many of the first results, while quite accurate, required the use of highly simplified equipment and measuring techniques. Consequently, mention will be made only of those most recent and more accurate experiments in this area of gaseous electronics. In particular, we will confine our references to those which deal with the capture of free electrons by certain electrophilic gas molecules.

One of the first papers to appear in the literature, which describes a method for determining the mobility of  $SF_6^-$  ions in the parent gas was that of McAfee<sup>1</sup> in 1955. During that time, the popularity of  $SF_6$  was increasing

rapidly because of its high electric strength, making it usable as an insulation medium in certain transformers and other electrical equipment. Sulfur hexafluoride ( $\text{SF}_6$ ) is representative of a class of halogen containing molecules which are of special practical interest because of their extraordinary ability to attach themselves to free electrons and form fairly stable negative molecular ions. Following the work of McAfee<sup>1</sup>, other investigators have carried out thorough investigations of electron attachment by certain molecules. For example, it has been shown<sup>2</sup> that direct capture occurs when the electron is near thermal energy in  $\text{SF}_6$ . Although many other gases have since been synthesized with even greater electron affinity, insufficient data are currently available in the literature to describe their electron capture characteristics with any degree of accuracy. Since  $\text{O}_2$  also forms an  $\text{O}_2^-$  ion at thermal energies, it too has been studied very carefully throughout the years. The most recently published information<sup>3</sup>, suggests that the  $\text{O}_2^-$  ion has the reduced mobility of approximately  $2.7 \text{ cm}^2/\text{volt sec}$  when measured in pure oxygen.

There are essentially two important mechanisms for the production of negative ions by electron impact. The most important of these is direct capture wherein a free electron is captured by a neutral molecule with the vibrational excitation of the molecular ion and its subsequent stabilization occurring during a collision with another molecule. A special case of direct capture is one in which stabilization is enhanced by an electron exchange process between the vibrationally excited molecular ion and another molecule of the same gas in a time short compared with the mean lifetime of the ion. It may also be possible to exchange the negative electron charge between unlike molecules. In such a case, the exchange favors the species with the lower ground state and longer lifetime.

A second, and less important mechanism for the formation of negative ions by the interaction of electrophilic molecules with electrons, is that known as dissociative attachment. In such a process, a free electron is captured by a neutral molecule and the excess energy causes dissociation of the molecule into two or more fragments, one of which is a stable negative ion. In both mechanisms, the initial attachment is a resonance process and occurs over a limited range of electron energies. The latter are usually in the thermal region.

As a result of our own research on the behavior of the electro-negative gases, as well as an examination of recent investigations dealing with electron attachment processes, we have developed an instrument which employs these phenomena for the detection and examination of the physical properties of negative ions produced by high molecular weight perfluorocarbon materials mixed with air. This instrument is, in many respects, analogous to that used

by Chanin, Phelps and Biondi<sup>3</sup> in their measurements of electron capture of  $O_2$  molecules. It does, however, differ in one important respect which will be described in detail in the sections which follow. In this report we describe the experimental method and demonstrate its feasibility as a technique for the examination of electron attachment characteristics by electronegative gases mixed with gases of low molecular weight.

It is the purpose of this report to show that certain electrophilic molecules of high molecular weight have strong tendencies to attach themselves to free electrons. Although most of the measurements have been made at room temperature, the results reported form a basis from which to demonstrate the quenching effect of the materials at re-entry temperatures. Contained also herein, are measurements of electric breakdown of some of the chosen electrophilic materials as a function of temperature. These results are presented in an effort to show that thermal effects are of importance and must be taken into consideration when considering electrophilics for the quenching of re-entry plasmas.

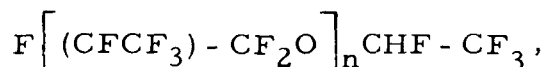
In the final portion of the report, we have introduced some of the data obtained by our technique into a hypothetical quiescent plasma in order to obtain an estimate of the densities of an electrophilic material required to reduce the electron concentration to a value which eliminates black-out. To be sure, these calculations cannot apply to re-entry conditions because we have employed experimental results which are only applicable at room temperature. They should, however, provide us with useful basic information for later use in more sophisticated re-entry calculations.

## SECTION II

### ELECTRON ATTACHMENT BY ELECTROPHILIC GASES

#### 2-1 Properties of Chosen Electrophilic Materials

A number of very high molecular weight perfluorinated materials have been considered for study under this contract. Throughout the course of the research, we were able to obtain samples of perfluorohexane, perfluoroheptane, perfluorooctane, *c*-C<sub>8</sub>F<sub>16</sub>O, Freon E-3, Freon E-4, and Freon-5. The general chemical formula for the members of the Freon E series may be written as follows;



where n represents the value of the number following E in the Freon series.

As a result of correspondence and telephone contacts with both the Minnesota Mining and Manufacturing Company and the E. I. DuPont de Nemours and Company, we have been able to gather a considerable amount of information regarding the physical properties of the materials referred to above. Of special significance, during this research effort, was the availability of vapor pressure data on all of the chosen electrophilics. This information is presented by plots of the logarithm of the vapor pressure as a function of the reciprocal of the absolute temperature in Figure 1. By use of such information, it is relatively easy for us to introduce known quantities of each material into our drift chamber (described below) at room temperature without depending upon an accurate indication of pressure by use of the differential manometer. Only in the cases of perfluorohexane, perfluoroheptane, perfluorooctane, and *c*-C<sub>8</sub>F<sub>16</sub>O have we been able to obtain an accurate reading of the pressure by the use of the manometer. For the other four materials the data in Figure 1 are essential in providing the necessary information regarding the quantity of material added to the air sample.

#### 2-2 Experimental Procedure for Electron Capture Measurements

##### 2-2-1 The Vacuum System

The vacuum system used under this contract consists of standard components such as bakeable valves, a bakeout oven a roughing pump with a

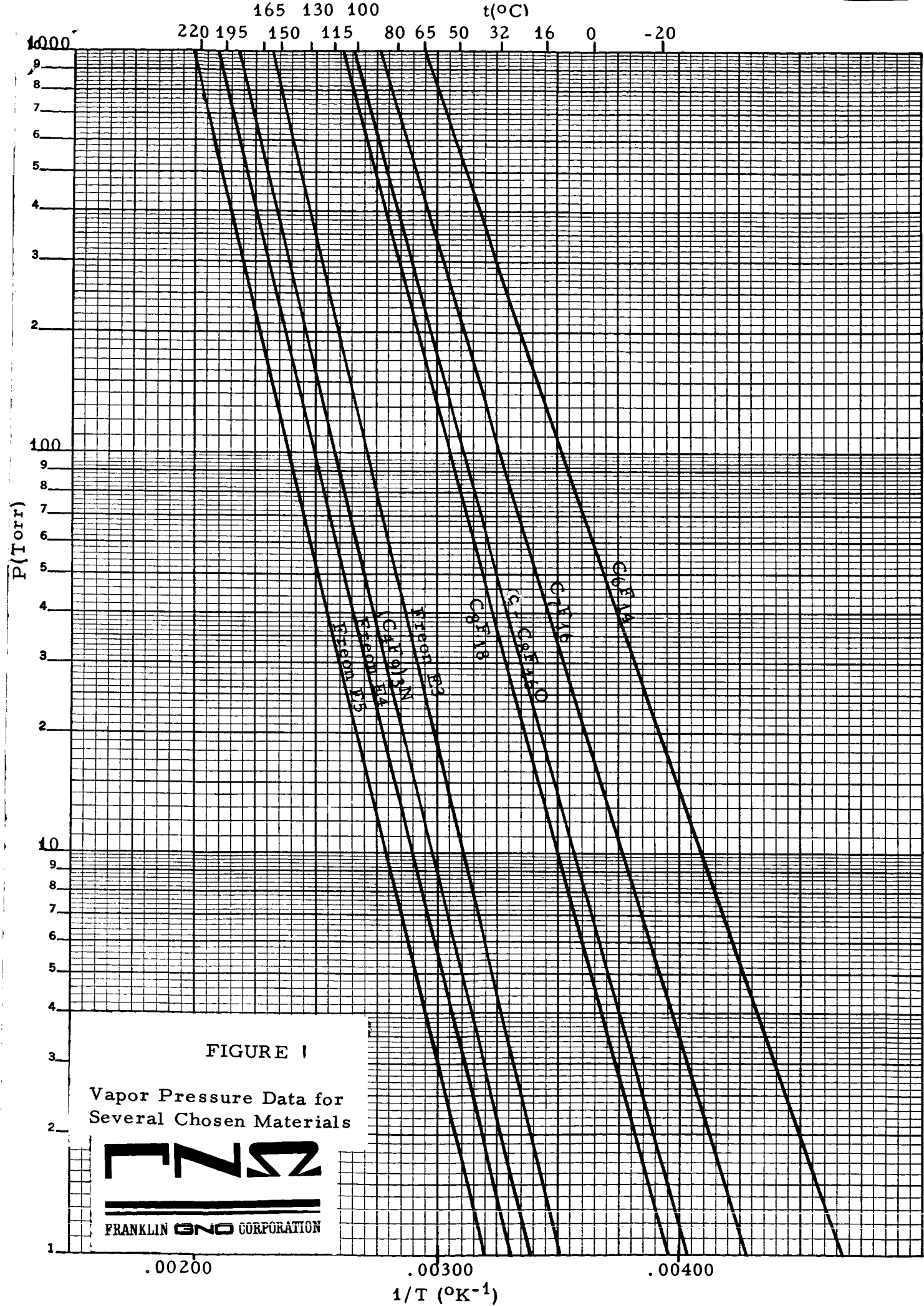


FIGURE 1

Vapor Pressure Data for  
Several Chosen Materials



thermocouple gauge indicator, and a VacIon pump. The latter is capable of reducing the pressure within the system to approximately  $10^{-8}$  Torr. The bakeout procedure as well as the attainment of a high vacuum is necessary in order to reduce contamination within the system to a minimum prior to the introduction of a sample for measurement. Such careful treatment of the system was found to be necessary when preparing the drift chamber for the introduction of a new electrophilic material following a previous set of measurements.

In order to measure the pressure of the gas within this system after bakeout, a Wallace and Tiernan differential manometer was employed. This instrument has been carefully calibrated prior to its installation. The case of the manometer is connected to the roughing line, and the capsule to the high vacuum portion of the system. Such an arrangement allows us to fill the high vacuum system to any desired pressure up to one atmosphere with a great deal of accuracy. A simple schematic block diagram of the entire vacuum portion of the apparatus is presented in Figure 2. Note that provision is made for introducing both a sample of the electrophilic material and the desired amount of air to be used as a working medium.

#### 2-2-2 The Drift Chamber

The measurements reported here were made by the use of a drift chamber consisting of a cathode, a series of guard rings, a pyrex envelope with a quartz window, a control grid, and a collector anode. This structure is essentially the same as that used earlier by Chanin, Phelps, and Biondi<sup>3</sup>. A highly simplified schematic diagram of the chamber is shown in Figure 3. The purpose of the guard rings is to insure a uniform electric field within the drift tube during measurement. The quartz window has been introduced to allow ultraviolet light to impinge upon the cathode surface to produce photoelectrons. The control grid consists of two sets of parallel wires with alternate wires connected electrically. This construction allows us to apply a bias voltage to control the flow of negative ions to the collector anode. All elements within the chamber are constructed of stainless steel with the exception of the grid wires. The latter are gold plated tungsten 2 mils in diameter.

#### 2-2-3 The Principle of Operation

The method employed in the present investigation differs in one important respect from that used by previous investigators<sup>3</sup>. This involves the method of application of the drift voltage. In the previous work, the drift voltage was applied constantly throughout each pulsing sequence. This method allows a considerable degree of attachment throughout the entire volume of the drift chamber because of the continuous distribution of electrons induced by the

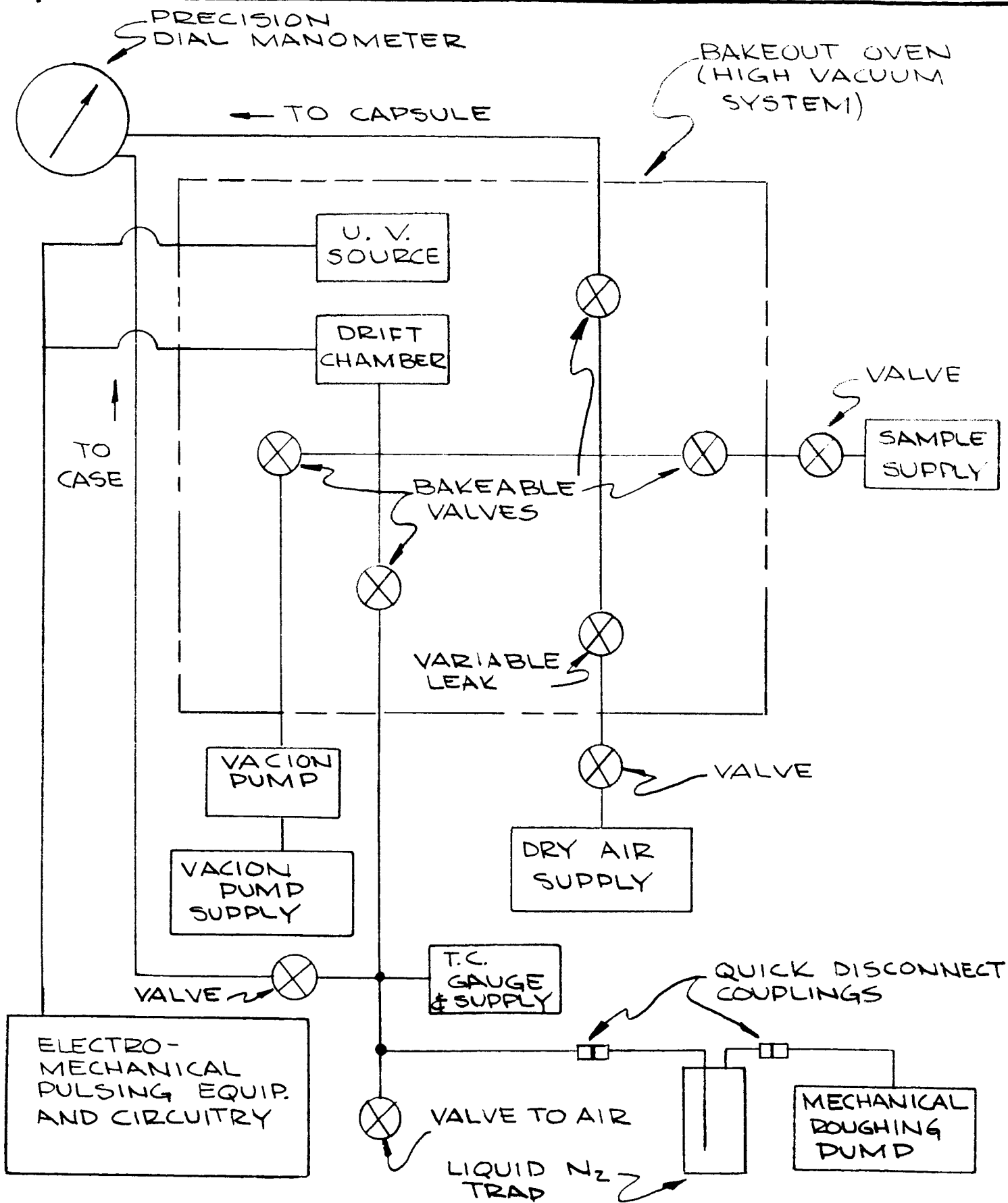
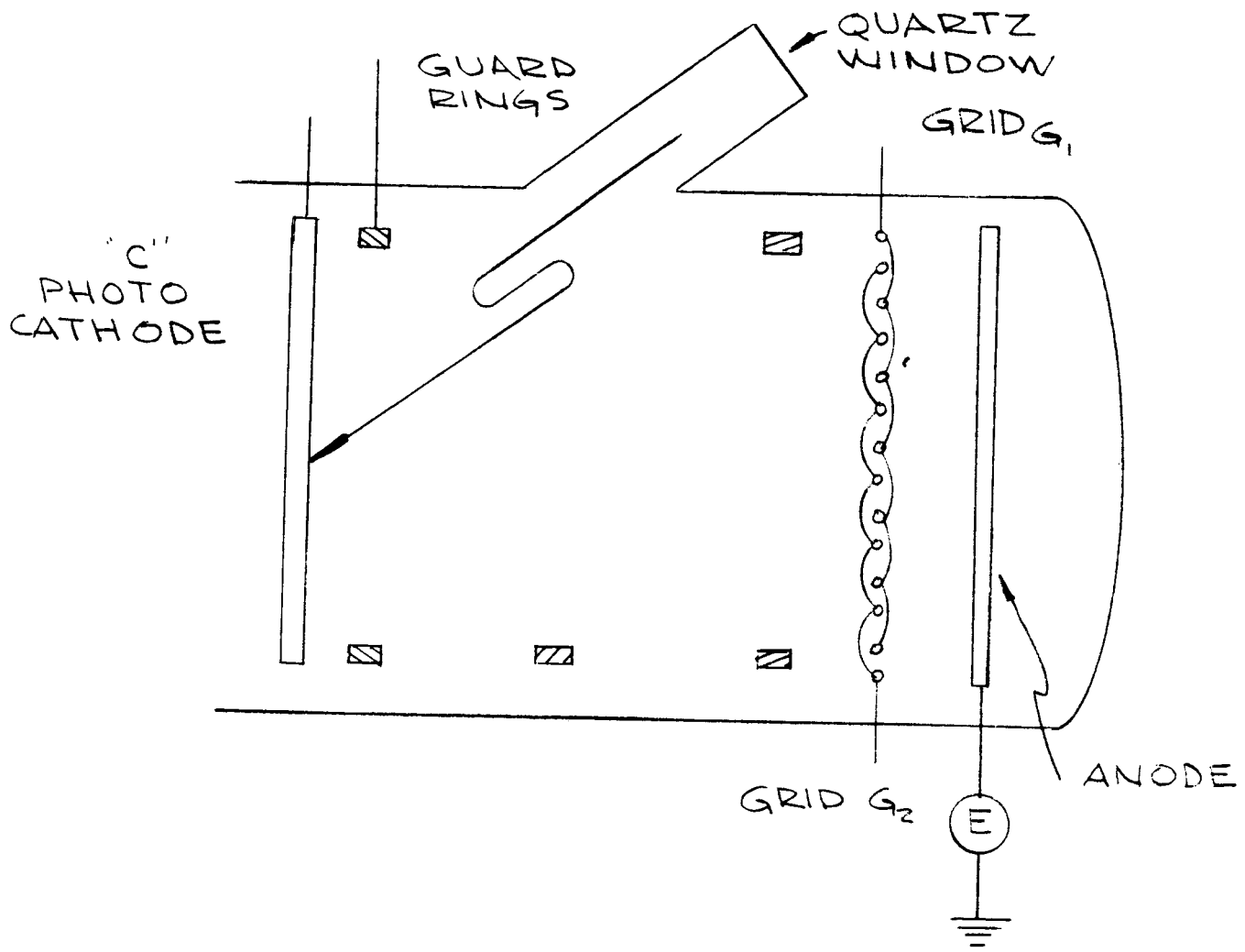


FIGURE 2	NUMBER
TITLE SCHEMATIC BLOCK DIAGRAM, VACUUM SYSTEM	





**FNS**  
 FRANKLIN GNO CORPORATION

FIGURE 3

NUMBER

TITLE SCHEMATIC DIAGRAM  
 OF  
 DRIFT CHAMBER

drift field between the cathode and control grid. The special control grid, which consists of thin parallel wires with alternate wires connected electrically, is kept closed with respect to transmission of both ions and electrons by the application of an equal and opposite bias voltage between adjacent wires. However, during selected evenly spaced time intervals, the grid is made transmitting by the application of rectangular voltage pulses which reduce the field between adjacent wires to zero and allow most of the ions and electrons to pass through to the collector anode. The pulses of current transmitted to the anode during the open intervals are integrated over a large number of cycles by an electrometer for this selected delay time interval. By making runs with various time delays, the ion current reaching the grid may be determined accurately as a function of time without measuring the grid current directly.

Although the former method<sup>3</sup> provides a considerable amount of information regarding the electron attachment characteristics of a single negative ion species in the gas improvements which we have made allow one to distinguish one mobility from another in a mixture of ionic species. The latter is accomplished by reducing the electric field between the cathode and control grid to zero during the time that the photopulse appears. Such a procedure should allow electron attachment to take place rapidly near the vicinity of the cathode during the photopulse with little or no attachment in the volume of the drift chamber. Electron attachment throughout the volume of the drift chamber should occur only as a result of the diffusive spreading of electrons in the field-free region.

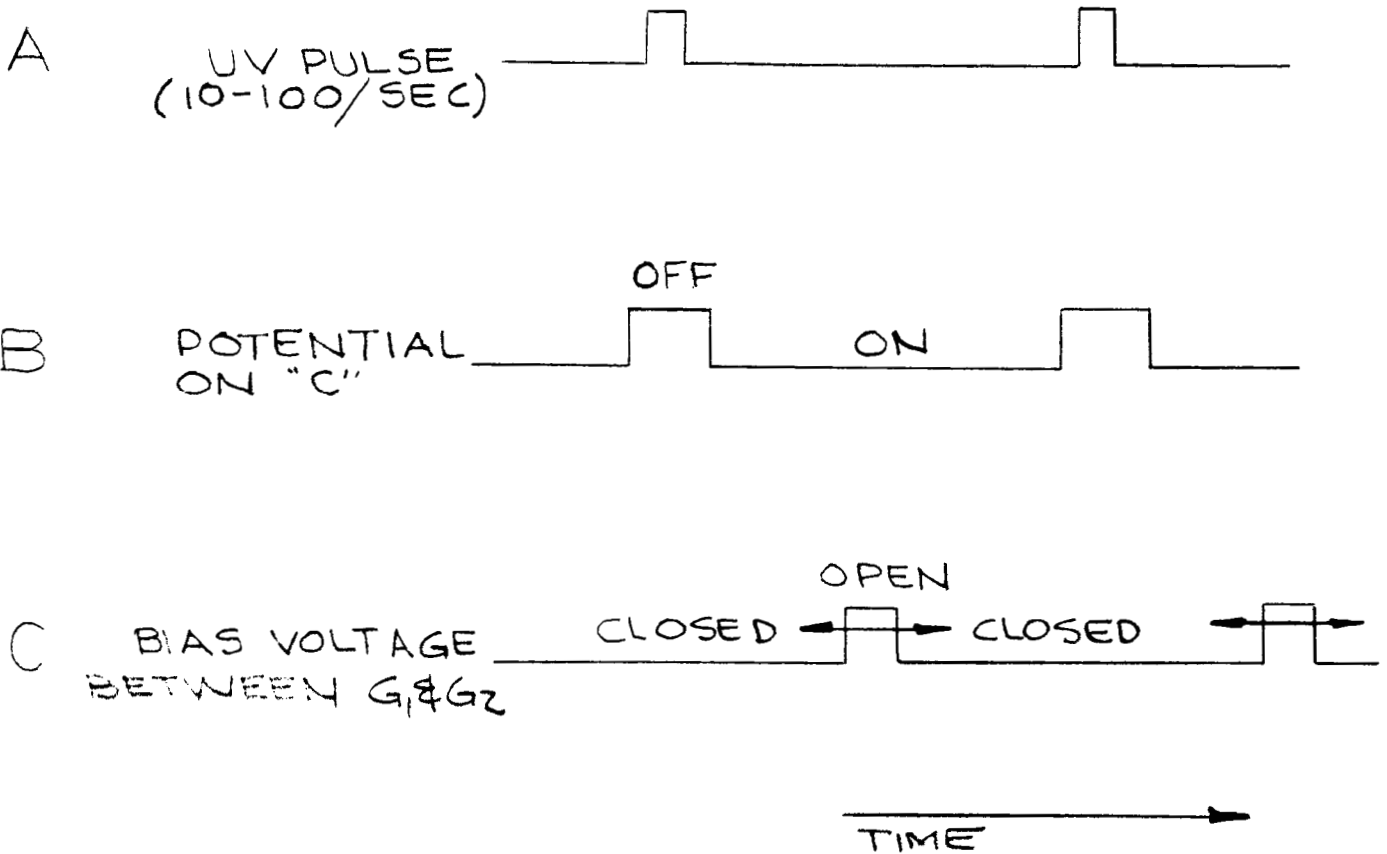
For the research conducted under the present contract, as in the previous work<sup>3</sup>, the control grid is normally closed to the passage of ions by the application of equal and opposite bias voltages to the adjacent wires, and is made to transmit for a short period of time which may be varied continuously throughout the pulsing sequence. The pulsing sequence is, however, adjusted in such a manner that mass selection is possible. This is accomplished primarily by the method of applying the drift voltage between cathode and control grid. Instead of supplying a constant drift voltage, the latter is pulsed in a particular relationship with the ultraviolet pulse which produces the photoelectrons. This allows the buildup of a very well defined ion pulse shape at a known location between the electrodes of the drift chamber.


Since the delay time can be varied continuously throughout each cycle of application of the photopulse, the net result of the pulsing sequence is that the electrometer will record the arrival of negative ions of different mobilities at the control grid. This, of course, results in the observation of the presence of negative ions of different mobilities in a gas which may contain more than one electrophilic component.

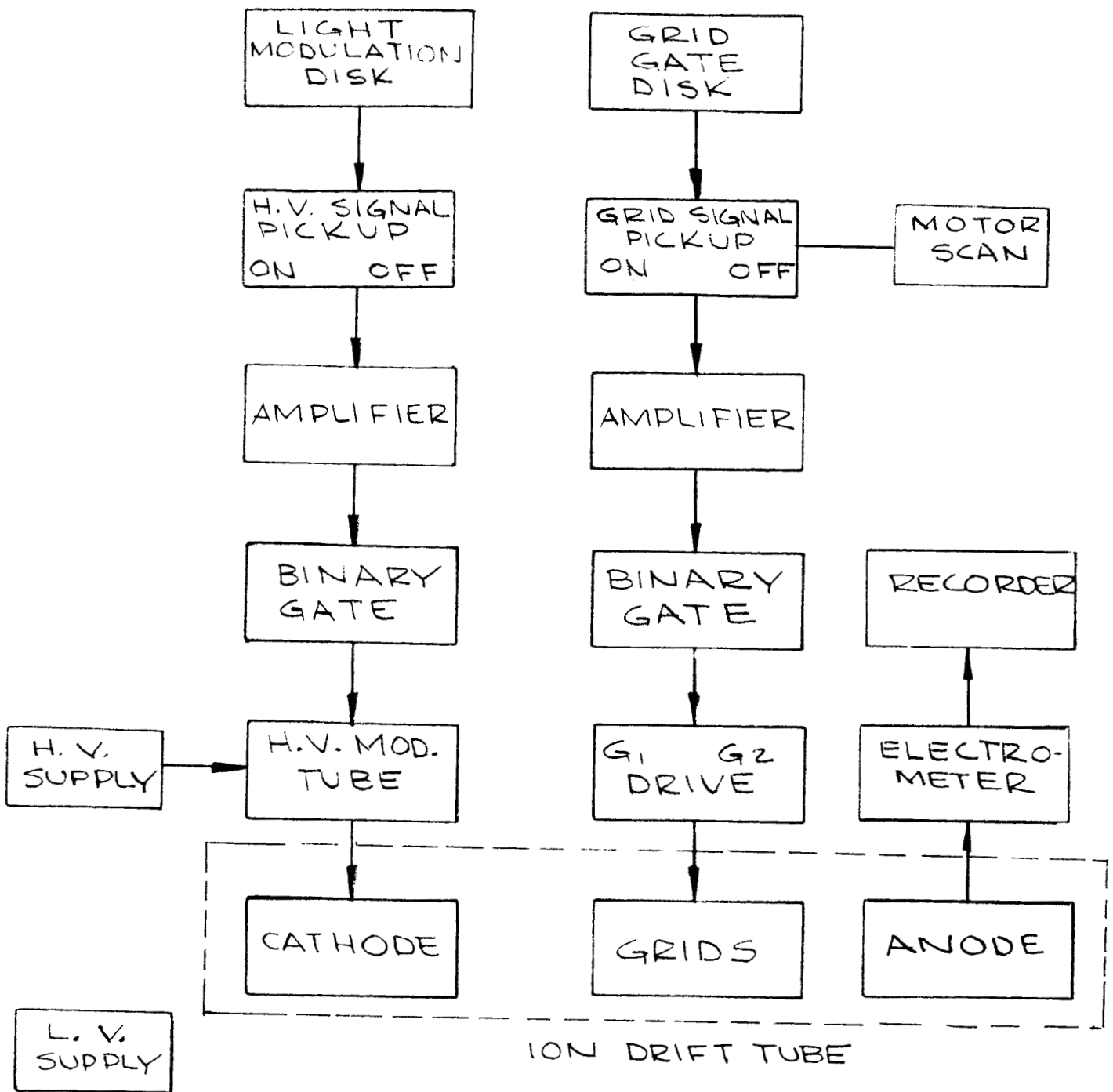
In Figure 4 we have presented a diagrammatic representation which provides a brief description of the pulsing sequence used for the present research. The upper curve marked A represents the sequence in terms of the pulsing of the ultraviolet source upon the surface of the cathode. In the curve B below, we represent diagrammatically the potential at the cathode surface as a function of time synchronized with the photopulse. To complete the picture, we have presented on the bottom curve marked C, the bias voltage between adjacent wires in the control grid as a function of time. The arrows indicate that the grid opening pulse may not only be varied in duration but may be scanned throughout the entire interval between light pulses. As ions of different mass traverse the distance between the cathode and control grid, the initial ion pulse should separate into distinct pulses which reach the control grid at different times. Consequently, we should expect to read integrated current pulses on the electrometer corresponding to each ion species within the gas mixture. The only requirement is that the time between light pulses be sufficiently long that all ions are capable of crossing the drift distance between pulses. If this is not possible, the data obtained will be confusing and of little or no value to us.

The method for producing light pulses of constant intensity has been achieved by the use of a rotating aluminum disc into which a slot has been cut. Also embedded in the disc are magnets which generate the necessary signals to be fed into the electronic circuitry to provide the desired pulsing sequence. The disc is driven by a variable speed motor so that the repetition rate of ultraviolet pulses can be varied at will. The ultraviolet source is a 20 watt deuterium lamp obtained from Bausch and Lomb. It is chosen as the source of photoelectrons because of its broad emission spectrum in the ultraviolet range from approximately 1900 to 3000 angstroms. Scanning of the grid bias pulse is achieved by the use of a 1/3 rpm motor driving a magnetic pickup. The latter interacts with a magnet carefully positioned on the rotating disc. The signal is then carried to the electronic circuitry to produce the desired grid pulse. Such a procedure allows complete scanning throughout the entire pulsing sequence. Additional magnets are embedded into the rotating disc, from which magnetic pickups feed signals into the electronic circuitry to produce the cathode pulsing as shown in curve B in Figure 4.


A system block diagram of the experimental assembly is shown in Figure 5. The system ground is located in the anode circuit to allow the electrometer to operate at ground potential. This dictates that all drift tube voltages be negative with respect to ground. One adjustable voltage dc power supply establishes the grid average potential, negative with respect to the anode, for the coplanar control grids in the drift tubes. Additional power supplies and dynamic circuits control the instantaneous potential of each grid



 <hr/> <b>FRANKLIN GNO CORPORATION</b>	FIGURE 4	NUMBER
	TITLE PULSING SEQUENCE FOR ATTACHMENT MEASUREMENTS	



NOTE: LESS VACUUM SYSTEM

 <p>FRANKLIN ENO CORPORATION</p>	FIGURE 5	NUMBER
	TITLE BLOCK DIAGRAM OF THE EXPERIMENTAL SYSTEM	

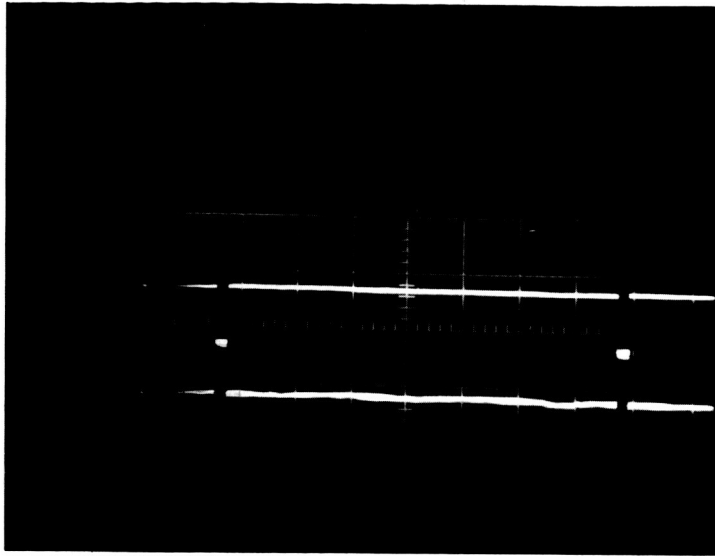
with respect to the grid average potential. A second adjustable voltage dc power supply applies a potential, negative with respect to the grid average potential, to the cathode of the drift tube. Additional power supplies and dynamic circuits control the instantaneous potential with respect to the grid average potential.

As mentioned earlier, the cathode is normally operated at the cathode average potential. During the time that the light impinges upon the cathode, the potential of the latter is switched to the grid average potential. At a controlled time following each pulse of light on the cathode of the drift tube, the grids are switched to the grid average potential for a short period of time. Normally, the grids are maintained at equal and opposite potentials from the grid average potential by virtue of the dynamic circuits.

The drift tube control circuitry is in this research effort basically a two channel system, where both channels are controlled from the rotating disc which generates the pulse of ultraviolet light on the cathode of the drift tube. As each magnet on the disc passes a pickup head, it generates a positive and negative going waveform which is synchronized with the pulse of ultraviolet light. The cathode drive channel consists of two bar magnets already mentioned, one which actuates the control channel just prior to the generation of the light pulse, and the other which energizes the channel just following the light pulse. The grid drive channel, however, uses only a single bar magnet and drives a one-shot circuit which generates a pulse of controllable width, which is independent of the speed of rotation of the modulation disc. In both circuits, the input signal from the pickup coil is amplified and used to fire a Schmitt trigger circuit into one of its two stable states. In the cathode drive channel, the output of the Schmitt trigger is used to trigger the input of the control binaries which divides the count by two. In turn, the output of the control binary is amplified and used to generate a cathode pulse which will drive the cathode from the cathode average potential to the grid average potential. In the grid drive channel, however, the output of the Schmitt trigger is used in parallel as an input to the control binary and to the one-shot timing circuit. At the completion of the one-shot timing, its output will trigger the control binary and, thereby, reset it for the next pulse. Following the control binary is a phase splitting push-pull amplifier which ultimately provides power to the potentials of the two control grids.

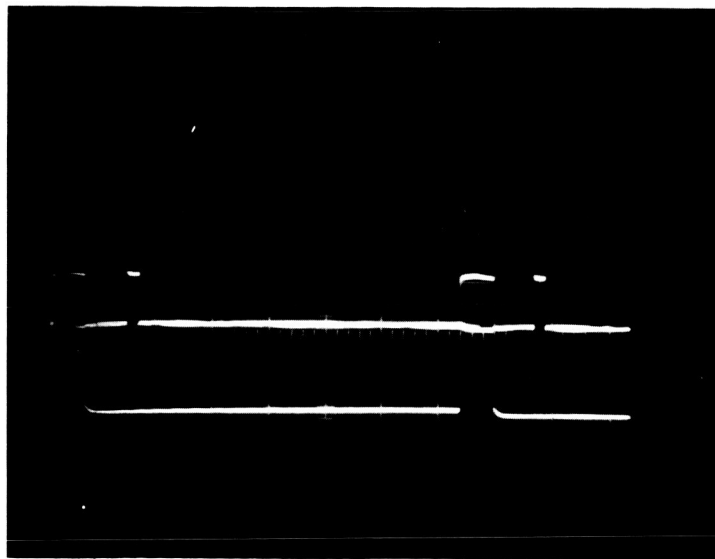
In order to provide a checkout of the system, we have employed a dual channel oscilloscope, and examined the characteristic outputs of the various elements making up the pulsing sequence. In Figure 6A is shown a simultaneous display of the bias pulsing sequence of the control grid. Note that pulsing of the grid reduces the potential difference between adjacent wires to zero. In Figure 6B is a simultaneous display of the cathode pulsing sequence with one grid pulse

(A)



Typical Grid Bias Pulsing Sequence.

(B)



Cathode Pulsing Sequence with Positive Grid Pulse Showing.

showing. Note that the potentials are equal when the cathode is pulsed off and the grid is open.

The oscillogram shown in Figure 7A is a simultaneous display of the cathode and photopulsing sequences. In order to examine the shape and position of the photopulse, it was obviously necessary to resort to somewhat more sophisticated techniques. This was accomplished by placing a small photodiode with a very rapid response directly in the center of the quartz window and connecting it to a small power supply.

A voltage indication provided an adequate representation of the intensity of the ultraviolet light as the slot in the rotating disc passed the quartz window. In order to provide verification that the potential between the cathode and control grid was indeed zero during the time that photoelectrons were being admitted, a single sequence in Figure 7A was expanded extensively and is shown in Figure 7B. It is clear from these results that no drift voltage was being applied during the time that the light was striking the surface of the cathode. Thus, we can say, from examination of Figure 6 and 7, that the sequence takes place in the proper manner.

#### 2-2-4 Calibration of Equipment

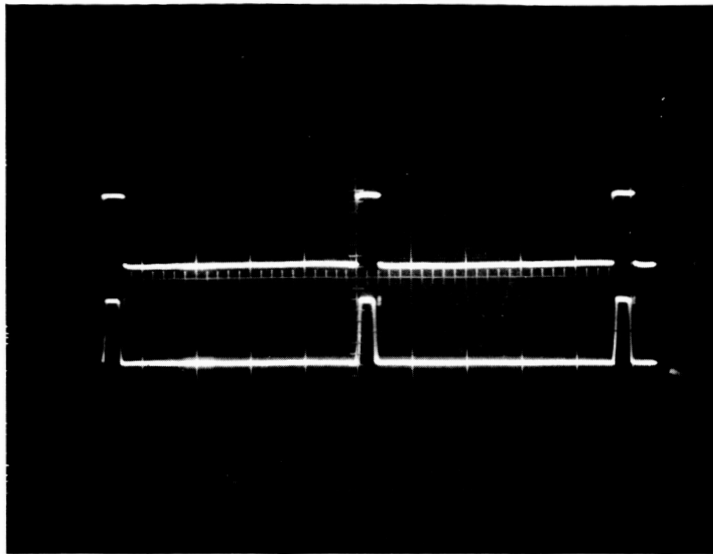
Before introducing the chosen electrophilic materials into the drift chamber for investigation of their electron attachment characteristics, it seemed advisable to calibrate the apparatus with a gas which is known to form negative ions and for which considerable information regarding its ionic mobility is available in the literature. The well-known electrophilic gas  $\text{SF}_6$  was chosen for this purpose. To aid in this effort, it was desirable to obtain a permanent record of the experimental results. This was accomplished by presenting the electrometer readout upon a suitable recorder.

We have found that a Leeds and Northrup recorder is satisfactory for this purpose. Experimental results presented in this manner make possible careful and accurate analysis of repeated measurements of electron attachment under various conditions of pressure and applied voltage. Visual observation of the electrometer current provides us with a hint regarding the arrival of a gaseous ion cloud at the control grid, but the permanent recorder tracing renders it possible to make various calculations associated with the observed results.

We have carried out a number of mobility determinations of the  $\text{SF}_6^-$  ion in pure  $\text{SF}_6$  at values of  $E/P$  (the ratio of the electric field to the gas pressure) varying from 0.6 to 1.2 volts/Torr cm. Information regarding sixteen of these individual measurements is tabulated in Table I. While there was some spread

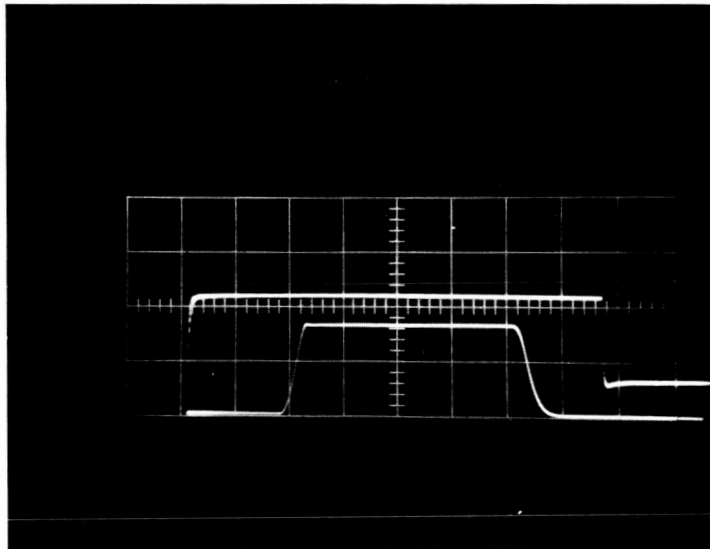


(A)



Cathode and Photo Pulsing Sequences measured Simultaneously. Cathode Pulse Shown on Upper Tracing.

(B)



Expanded Oscillogram of Above Sequences Showing Single Cathode Pulse and Photo Pulse.

FIGURE 7

TABLE I

RESULTS OF MOBILITY MEASUREMENTS OF SF<sub>6</sub><sup>-</sup> IN SF<sub>6</sub>

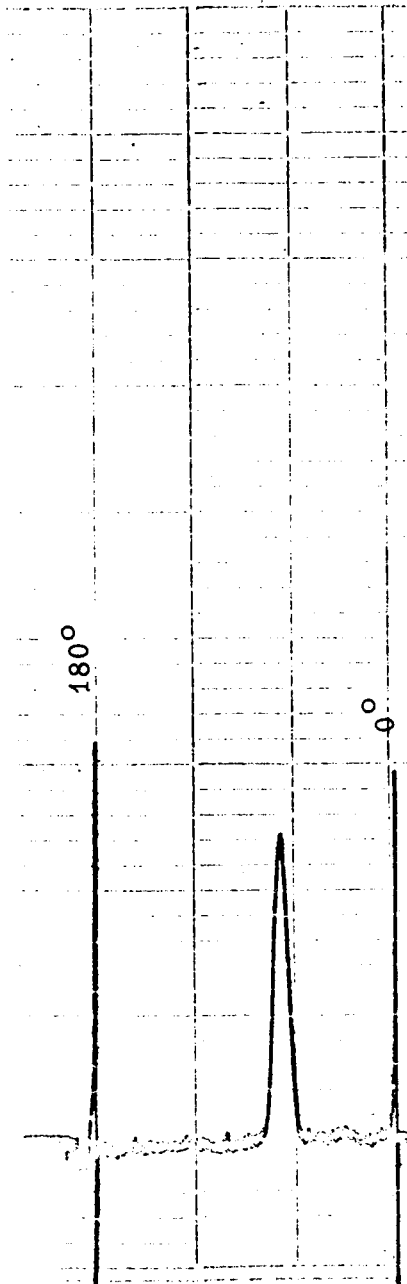
V Appl.	E(Volts/cm)	P(Torr)	E/P	v <sub>d</sub> (cm/sec)	μ <sub>o</sub>
110	15	12.7	1.2	600	.668
110	15	12.7	1.2	608	.677
110	15	12.7	1.2	561	.625
110	15	12.7	1.2	562	.626
110	15	12.7	1.2	561	.625
110	15	12.7	1.2	598	.666
40	5.5	5.1	1.1	487	.594
40	5.5	5.1	1.1	406	.495
40	5.5	5.1	1.1	429	.523
110	15	25.4	0.6	281	.626
110	15	25.4	0.6	281	.626
190	26	25.4	1.0	521	.670
190	26	25.4	1.0	521	.670
110	15	25.4	0.6	270	.601
110	15	25.4	0.6	292	.651
110	15	25.4	0.6	270	.601
				Avg.	0.621
			Literature Value		0.570

in the measured value of the reduced mobility  $\mu_0$ , the average value obtained was equal to  $0.62 \text{ cm}^2/\text{volt sec}$ . This value may be compared with the most recent literature value of  $0.57 \text{ cm}^2/\text{volt sec}$ .<sup>4</sup> The agreement is sufficiently accurate to indicate that our method of measurement is reliable. (See Figure 8).

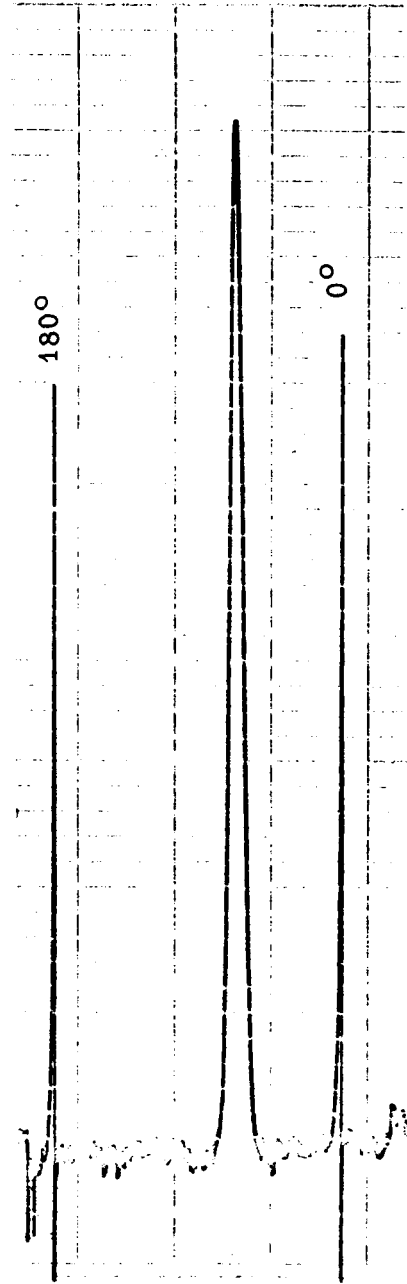
In order to provide a typical example of one of the experimental observations made during the calibration, we present two recorder tracings of the integrated electrometer current as it is observed (see Figure 8). These tracings show that there is a sharp, well-defined current peak at a given position of the scanning arm relative to the application of the drift voltage. As will be clarified later, the relationship between this position and the time required for the ion cloud to traverse from the cathode to the control grid is easily calculable. The reason for showing these two recordings is twofold. In the first place, they show that the spatial distribution of charges in the  $\text{SF}_6^-$  ion cloud is indeed a narrow one. Of even greater importance, however, is the fact that the output of the electrometer is completely linear at these low current ranges. There is, of course, a small background noise which is almost impossible to avoid at these highly sensitive ranges. Further investigations have shown that operation of the electrometer is linear down to the  $10^{-13}$  ampere full scale setting. In Figure 8,  $t_0$  represents the time between the pulsing sequences,  $t_g$  is the duration of the grid bias pulse,  $V_{GK}$  is the applied drift voltage between cathode and control grid, and  $\mu_0$  is the reduced mobility of the  $\text{SF}_6^-$  ion as calculated from the information presented by the recordings.

#### 2-2-5 Calculations of Ion Pulse Dimensions

Experimentally, when a pulse of electrons (caused by pulsed photon exposure) diffuses from a plane through an electronegative gas, an electron density  $N_e(x, y, z, t)$  will be established at time  $t$  in a volume element  $dV = dx dy dz$ . There are three important times to consider in the derivation of a quantitative expression for  $N_e$ ; the electron pulse width or photon exposure duration ( $t_1$ ), the time of observation ( $t$ ) at  $dV$ , and the attachment time ( $1/Z_a$ ). The reason for the distinct time zones is coupling or interdependence between the density controlling processes. It is preferable to derive a general expression where  $t_1 \approx t \approx 1/Z_a$  so that no time is small compared with the other. Here  $Z_a$  is the attachment frequency, discussed in greater detail below.



Electrometer Range -  $.01 \times 10^{-10}$   
amps full scale



Electrometer Range -  $.003 \times 10^{-10}$   
amps full scale

Gas - Pure  $\text{SF}_6$   
 Pressure - 12.7 Torr  
 Motor  $t_0$  - .060 sec./rev.  
 $t_g$  -  $1.2 \times 10^{-3}$  sec.  
 $V_{GK}$  - 110 Volts  
 $\mu_0$  -  $.62 \pm 0.2 \text{ cm}^2/\text{volt sec.}$

Using Fick's law for diffusion, and treating the electrons as a gas without charge, where  $N_e$  is electron density and  $\underline{J}$  is electron current density in particles/cm<sup>2</sup>/sec.,

$$\underline{J} = -D \underline{\nabla} N_e. \quad (2-1)$$

Also using the equation for continuity,

$$\frac{\partial N_e}{\partial t} + \underline{\nabla} \cdot \underline{J} = 0, \quad (2-2)$$

then the time-dependent diffusion equation

$$\frac{\partial N_e}{\partial t} = \underline{\nabla} \cdot (D \underline{\nabla} N_e) \quad (2-3)$$

expresses a general relationship between electron particle density  $N_e$ , the diffusion coefficient  $D$ , and time.

The general expression shown in equation (2-3) is satisfied by the one dimensional Einstein density distribution<sup>5</sup>

$$N_e = (n_0 / \sqrt{4\pi Dt}) \exp - (x^2/4Dt). \quad (2-4)$$

The boundary conditions for this distribution are:

$n_0$  = the number of electron particles all located at the origin of a one-dimensional (x) coordinate system at  $t = 0$ .

$t$  = 0 when electron diffusion starts in the gas

$N_e$  = electron density at (x, t) in volume element dx.

2-2-5-1 Case I;  $t_1 \ll t, t_1 \ll 1/Z_a$ 

The simplest case to consider is when the electron pulse duration is much less than the time at which observations are made at volume element  $dx$ ; i. e., when  $t_1 \ll t$ . For this case, there is essentially no diffusion to be considered during the electron pulse. Therefore, the initial intensity ( $n_0$ ) is proportional to the "on-time"  $t_1$  of the photon exposure.

If the electron particle flux as particles/cm<sup>2</sup>/sec. ( $J$ ) is expressed in terms of electron current ( $i_0$ ), then we may write that

$$J = i_0/q, \quad (2-5)$$

and

$$n_0 = i_0 t_1/q, \quad (2-6)$$

where  $q$  is the electron charge.

Combining these equations, the electron density in volume  $dx$ , due to both photon exposure and diffusion becomes

$$N_e = (i_0 t_1/q \sqrt{4\pi Dt}) \exp - (x^2/4Dt), \quad (2-7)$$

$$t_1 \ll t$$

$$Z_a = \infty,$$

If attachments are allowed in the volume  $dx$ , and if the rate of attachment varies with both electron density and  $1/Z_a$ , then

$$N_e = (i_0 t_1/q \sqrt{4\pi Dt}) \exp - \left[ (x^2/4Dt) + Z_a t \right] \quad (2-8)$$

$$t_1 \ll t$$

$$t_1 \ll 1/Z_a$$

This equation assumes that electronegative molecules are not depleted significantly by attachment.

A typical graph (Figure 9), follows. It shows that at  $x = 0$ , the electron density generally decreases with time, and that longer photon exposures result in higher electron densities. Each of these curves is terminated at  $t = t_1$ , because diffusion within the pulse time has not been considered.

General conditions for the calculations are:

$$\begin{aligned}
 P_N &= 10^{-3} \text{ Torr for electrophilic gas component} \\
 P_B &= 760 \text{ Torr for the background gas} \\
 Z_a &= 10^4 \text{ events/sec.} \\
 D &= 66 \text{ cm}^2/\text{sec.} \\
 i_o &= 10^{-10} \text{ amperes due to photon exposure}
 \end{aligned}$$

2-2-5-2 Case II;  $t_1 \approx t \approx 1/Z_a$

For this case, photoelectric emission occurs continually during the time of observation at the volume element  $dx$ . That is to say, there is continuous electron emission.

Continuous emission is represented by the expression

$$n_o = \int_0^t (i_o/q) dt. \quad (2-9)$$

If all other processes are represented as in 2-2-5-1 then the general expression for electron density with continuous emission becomes

$$N_e = (i_o t/q \sqrt{4\pi Dt}) \exp - \left[ x^2/4 Dt + Z_a t \right]. \quad (2-10)$$

This equation of course is based on assumptions of dilute concentrations, constant values of  $Z_a$  and  $D$  over the time  $t$ , and no space charge considerations.

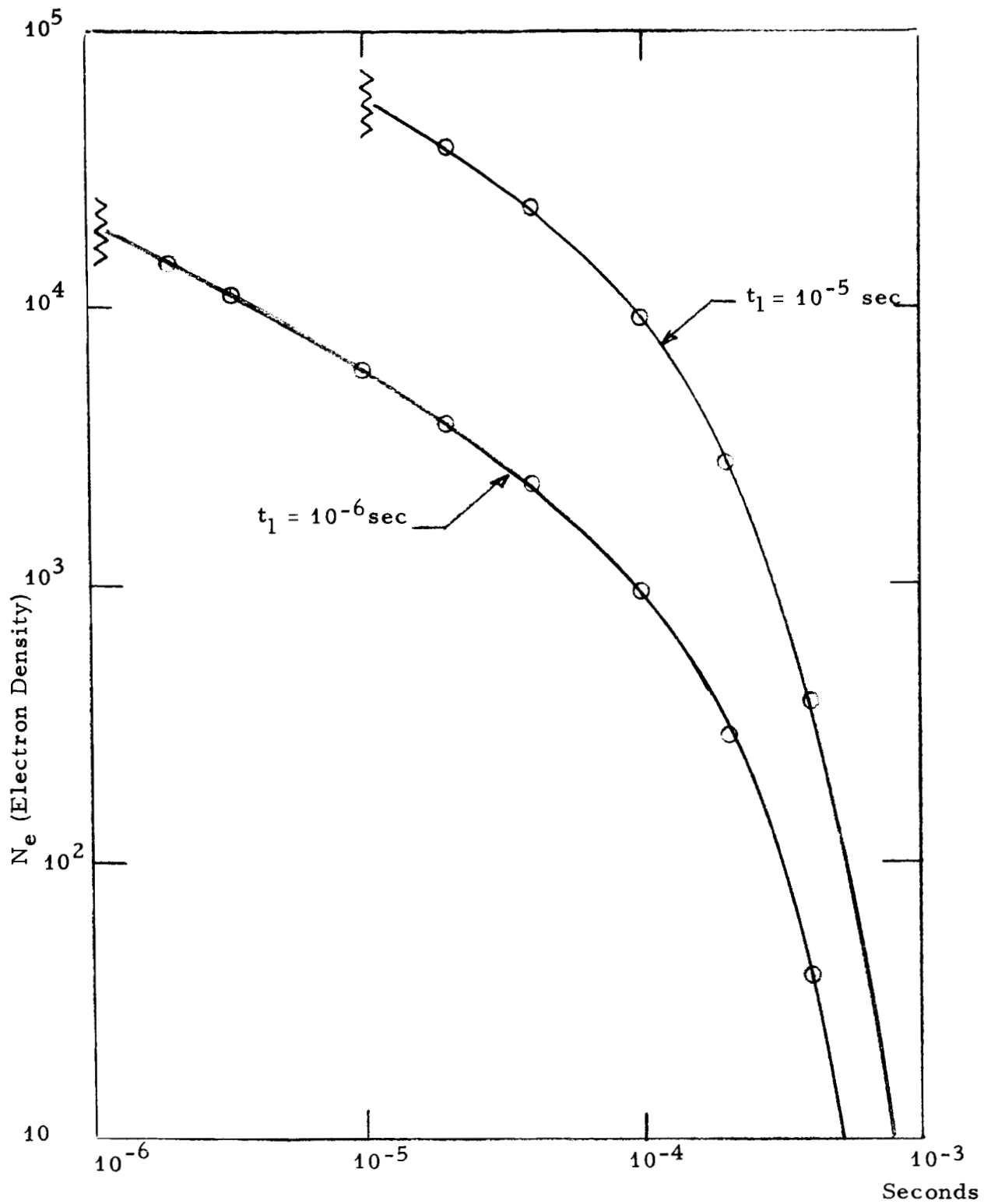


Figure 9

Calculated Electron Density at  $x = 0$  and Different Pulse Length,  $Z_a = 10^4/\text{sec}$ .



A much more general approach to the evaluation of  $N_e$  would be to use the time-dependent diffusion equation (equation 2-3)) modified for emission boundary values and space charge effects. However, for short times, where  $t_1 \cong t \cong 1/Z_a$ , the general behavior exhibited by this equation is satisfactory to point out the relative magnitudes of  $x$  and  $t$  which are suitable for the drift tube measurements described in the text of the report.

This approximate equation (equation (2-10)) for  $N_e$  breaks down as shown in the attached curves (see Figure 10) because electron densities eventually decrease with increasing exposure time. This is due to treatment of  $Z_a \cong 10^{-4}/\text{sec}$ . However, it is very clear that for pulses up to  $10^{-4}$  sec. duration, the major part of electron attachment will occur near the cathode at distances approximately 0.2 cm or less for the general conditions:  $D = 66 \text{ cm}^2/\text{sec}$ .,  $Z_a = 10^{-4}/\text{sec}$ ., and  $i_0 = 10^{-10}$  amperes. It is also clear that the electron densities are greater for the present case than for the situation in 2-2-5-1, as expected for the increased exposure time.

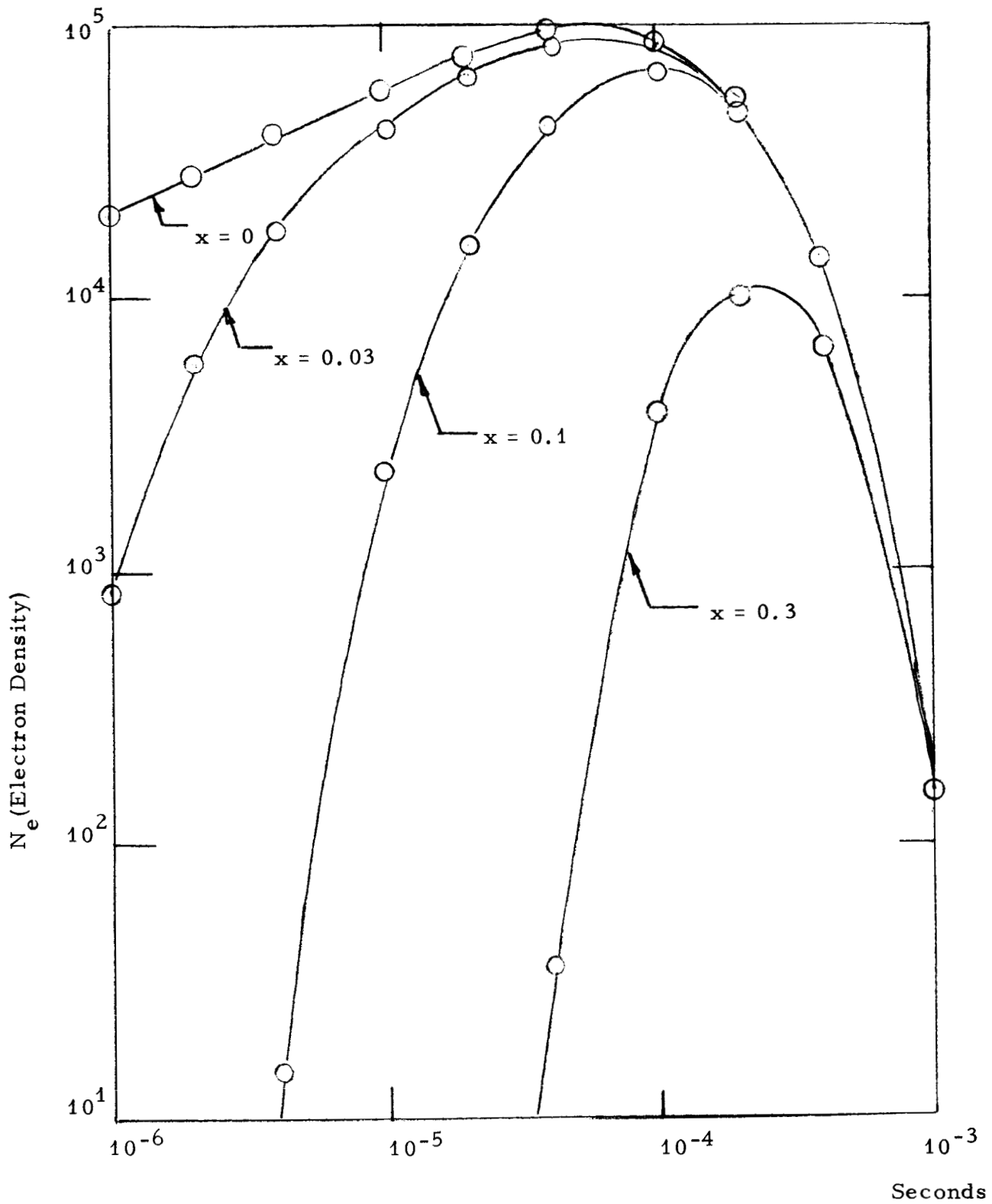


Figure 10

Calculated Electron Density Distribution  
 For Continuous Emission,  $Z_a = 10^4/\text{sec}$ .

## 2-3 Experimental Observations of Electron Attachment

After having successfully calibrated the equipment employed in this research effort, we were in a position to determine the feasibility of the method for the detection and examination of negative ions produced in the chosen electrophilic materials by electron capture. In particular, it was our desire to accomplish this by making measurements of electron capture by the electrophilic material mixed with air as the working medium. It was necessary to examine the electron capture characteristics of the materials specified in Section 2-1 above, and to provide a more detailed presentation of the meaning of the experimental observations obtained.

### 2-3-1 Method for Analyzing Data of Electron Capture

Throughout various portions of this report, reference will be made to recorder tracings obtained by our experimental technique using the attachment drift chamber. However, prior to presenting data in this form, we feel that it is desirable to provide a description of these tracings in terms of the physical phenomena which are occurring within the drift chamber. Such a description should be of value to the reader as an aid to interpreting the experimental observations. In this and following sections of the report, an effort is made to point out those physical parameters which can be deduced as a result of the drift chamber measurements. As a result, we can make decisions regarding desirable improvements in experimental techniques.

### 2-3-2 Typical Recorder Tracings

In most of the typical recorder tracings, which we have obtained by experimental measurement, it will be noted that the recorder pen exhibits a sharp spike at the point indicated by  $0^{\circ}$ , and then returns to an almost constant value for some time. This is followed by an increase and subsequent decrease of the integrated current measured by the electrometer to approximately the same value as before (see Figure 8). It is this peak which is characteristic of the negative ions produced by attachment processes in the vicinity of the cathode, modified as they approach the control grid. The second current spike, indicated in degrees, is used to indicate the completion of an experiment. The reason for the appearance of the current spike at the beginning and termination of an experiment is the result of switching surges in the line, which occur as the scanning motor is switched on and off respectively. They are used to advantage by providing an accurate indication of the time boundaries for each scanning experiment. Typical examples of such recordings will be reproduced later in this report.

2-3-3 Significance of Ion Peaks

Now let us direct our attention to the meaning of such observations as those described in the last section. First, let us define a number of physical parameters which are of importance. We will define  $n_i$  as the instantaneous one dimensional concentration of ions in the ion pulse traveling with a drift velocity  $v$  toward the control grid, and under the influence of a uniform electric field. For an actual situation in which the period between light flashes is equal to  $t_o$ , the control grid is open only for a small period of time  $t_g$  sec., so that the measured electrometer current  $i_m$  will follow the relationship:

$$i_m = n_i e v t_g / t_o . \quad (2-11)$$

The total charge within the ion pulse  $Q$  is, by definition:

$$Q = e \int_0^{\delta} n_i dx . \quad (2-12)$$

The combination of this with equation (2-11) gives the expression:

$$Q = (t_o / t_g) \int_0^{\delta} i_m dx / v . \quad (2-13)$$

In view of the fact that  $dx = v dt$ , equation (2-13) may be written as:

$$Q = (t_o / t_g) \int_0^{t_o} i_m dt . \quad (2-14)$$

As indicated above, the latter is a measure of the total number of ions produced by electron capture per photopulse between cathode and control grid.

2-3-3-1 Ion Mobility

The most obvious parameter which is made available from the attachment measurements which we make is, of course, the drift velocity or mobility of the ion or ions produced during the pulsing sequence. This information is obtained directly from the recorder tracings by the following methods. We provide a continuous monitor of the rate of the pulsing sequence by the use

of an oscilloscope. In most cases we have found it practical to use the value of  $t_o$  of 0.06 seconds. This is sufficient time for the ions with which we deal to traverse the space between the cathode and control grid. From an examination of the chart speed, and the rate of scanning, exactly 3 inches of chart paper correspond to one pulsing sequence. Thus we may say that each division (one-half inch) on the chart paper corresponds to 10 milliseconds of time, and we can readily equate distance to time as required. We have, therefore, a direct measure of the time required for the ion pulse to traverse the space between cathode and control grid. From this information, the mobility of the ion can easily be calculated.

### 2-3-3-2 The Photopulse

In order to make the results more meaningful, it is of interest to relate equation (2-14) to the total charge produced by the photopulse  $Q_o$ . If it can be assumed that the photocurrent produced during each individual photopulse is identical to that produced with the grid open under dc conditions, then  $Q_o$  can be expressed by the simple form:

$$Q_o = i_o t_1, \quad (2-15)$$

where  $i_o$  is the dc photocurrent and  $t_1$  is equal to the time between opening and closing of the slit (slightly less than the time that the light was allowed to impinge the cathode surface). While we realize that this is not the actual experimental condition, intuition leads us to believe that the true value of  $Q_o$  will be unaffected by the rise and fall of  $i_o$  as the light source enters and leaves the slot in the rotating disc. Since the drift cell aperture is circular, and the slit is rectangular, it is of interest to assure ourselves that the assumption is a valid one. This is easily done from the knowledge of the area of a segment of a circle, which is given by the expression:

$$A(y) = (\pi r^2 / 2) - \left[ y \sqrt{(r^2 - y^2)} + r^2 \arcsin (y/r) \right] \quad (2-16)$$

In the above expression,  $r$  is the radius of the circle and  $y$  is the perpendicular distance of the chord from the center of the circle. If we made the assumption that the distance  $u$  between the circumference of the circle and the chord is equal to  $r - y$ , equation (2-16) reduces to:

$$A(u) = (\pi r^2 / 2) - \left[ (r-u) \sqrt{(2r-u)u} + r^2 \arcsin (1-u/r) \right] \quad (2-17)$$

From the above,  $Q_o$  in equation (2-15) may be written by use of the following relationship;

$$Q_o = i_o \left[ (2/A_o v) \int_0^{2r} A(u) du + t_m \right]. \quad (2-18)$$

where  $v$  is the velocity of the circle relative to the rotating disc,  $A_o$  is equal to the total area of the circle, and  $t_m$  is the time that the entire circle is within the confines of the slit. We must assume here, of course, that the dimensions of the slit are large compared with those of the circle. We have solved equation (2-18) by numerical methods, and have obtained the same results as those given by equation (2-15). Thus, our intuitive assumption was an accurate one.

Previous experience with the measurement of photocurrents in gases has shown that  $i_o$  is unpredictable with time until the latter approaches several seconds. Furthermore, it must be remembered that during operation of the equipment, the drift voltage is not applied throughout the duration of the light pulse. This being the case, it is better to define  $Q_o$  in terms of an average photocurrent  $i_a$  as measured under experimental conditions with the control grid open. That is to say:

$$Q_o = (t_o/t_1) \int_0^{t_1} i_a dt = i_a t_o. \quad (2-19)$$

### 2-3-3-3 The Meaning of $Q/Q_o$

By the combination of equation (2-14) with equation (2-19), it becomes a simple procedure to obtain the ratio  $Q/Q_o$ . This relationship may be expressed as follows:

$$Q/Q_o = (1/i_a t_g) \int_0^{t_o} i_m dt. \quad (2-20)$$

This ratio gives the fraction of the electrons attached by a single photopulse as they traverse the distance between cathode and control grid. Since we are performing our experiments on materials with very high anticipated electron capture cross sections, it would be somewhat surprising not to observe a value of  $Q/Q_o$  close to unity in all cases. Indeed, failure of such observations would render the experimental procedure somewhat suspect.

#### 2-3-3-4 Typical Calculations

The choice of a convenient value for  $t_0$  makes possible an accurate determination of  $Q$ . Since we can equate  $\frac{1}{a}$  current of 1 ampere to  $6.3 \times 10^{18}$  unit charges/sec., data such as those shown in Figure 11 can be replotted as unit charges/sec. versus time in seconds. The area under the curve gives us the numerical value of  $Q$ . The first curve in Figure 11 is represented in this manner in Figure 12, in order to supply an example of the procedure. A polar planimeter is used to determine the area in question.

#### 2-3-4 Experimental Results Obtained

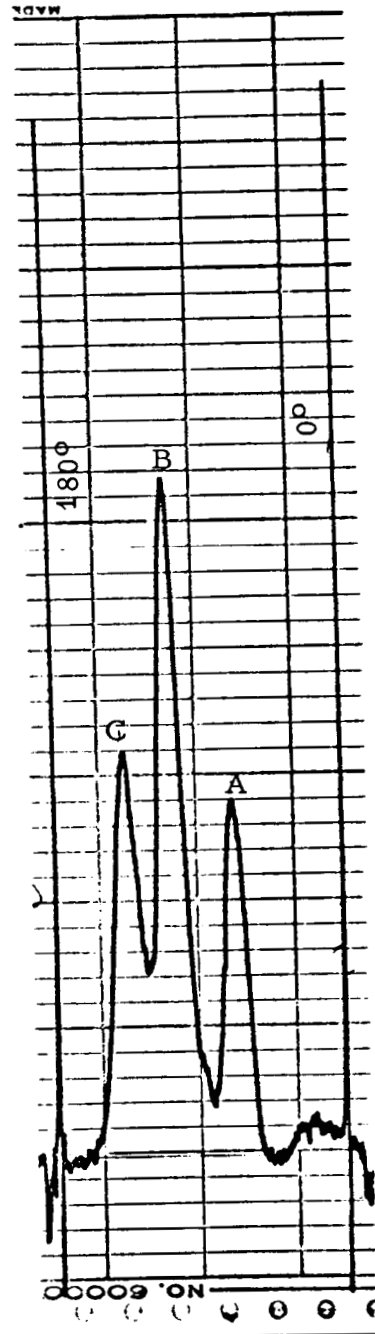
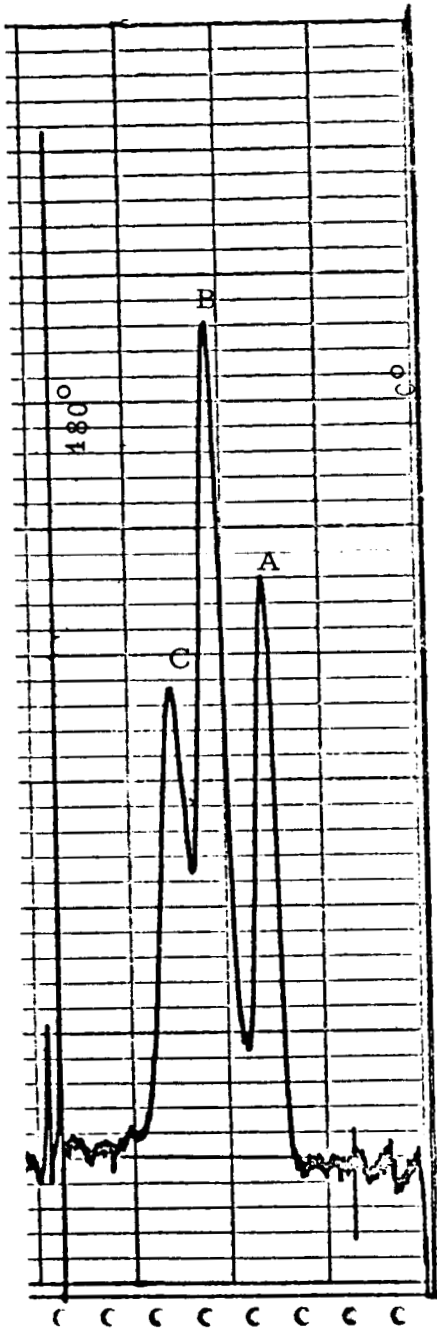
In order to obtain meaningful experimental results, it seems reasonable to assume that the total area encompassed by the tracing of ion peaks by the recorder must provide us with a measure of the total number of negative ions produced within the drift chamber by the photopulse (see Section 2-3-3).

The attachment characteristics of an electrophilic component in a working medium are, of course, directly related to both the total efficiency of ion production and the concentration of that component.

If the statement made in the last paragraph is to be valid, a number of requirements must be stipulated. For example, the duration of the control grid pulse must be maintained at a constant value which is much less than that of the true ion pulse. Secondly, the electrometer must measure accurately the integrated current of charge carriers as they approach the control grid. It is also desirable to apply an electric field between cathode and control grid of sufficient magnitude such that the dc photocurrent will be relatively insensitive to its value.

#### 2-3-4-1 Additional Improvements Made in Electronic Components

Until very recently, we had assumed that the electrometer was measuring a true integrated current, and that no changes would be required to correct its faulty behavior. The units being used in this research effort is a Model 610 BR Keithley instrument. During the latter part of March of this year, its operation was examined by our electronics group, and it was found necessary to make a number of corrections.



Gas Mixture -

24.1 Torr Air

1.27 Torr  $C_7F_{16}$

- $\mu_0$  Peak A -  $1.5 \pm 0.2$  cm<sup>2</sup>/volt sec.
- $\mu_0$  Peak B -  $.9 \pm 0.2$  cm<sup>2</sup>/volt sec.
- $\mu_0$  Peak C -  $.6 \pm 0.2$  cm<sup>2</sup>/volt sec.

Gas Mixture -

22.9 Torr Air

2.54 Torr  $C_7F_{16}$

- $\mu_0$  Peak A -  $1.0 \pm 0.2$  cm<sup>2</sup>/volt sec.
- $\mu_0$  Peak B -  $.6 \pm 0.2$  cm<sup>2</sup>/volt sec.
- $\mu_0$  Peak C -  $.5 \pm 0.2$  cm<sup>2</sup>/volt sec.

Electrometer Range -  $.003 \times 10^{-10}$  amps full scale

Motor  $t_0$  - .060 sec./rev.

$V_{GK}$  - 145 volts

$t_g$  -  $1.7 \times 10^{-3}$  sec.

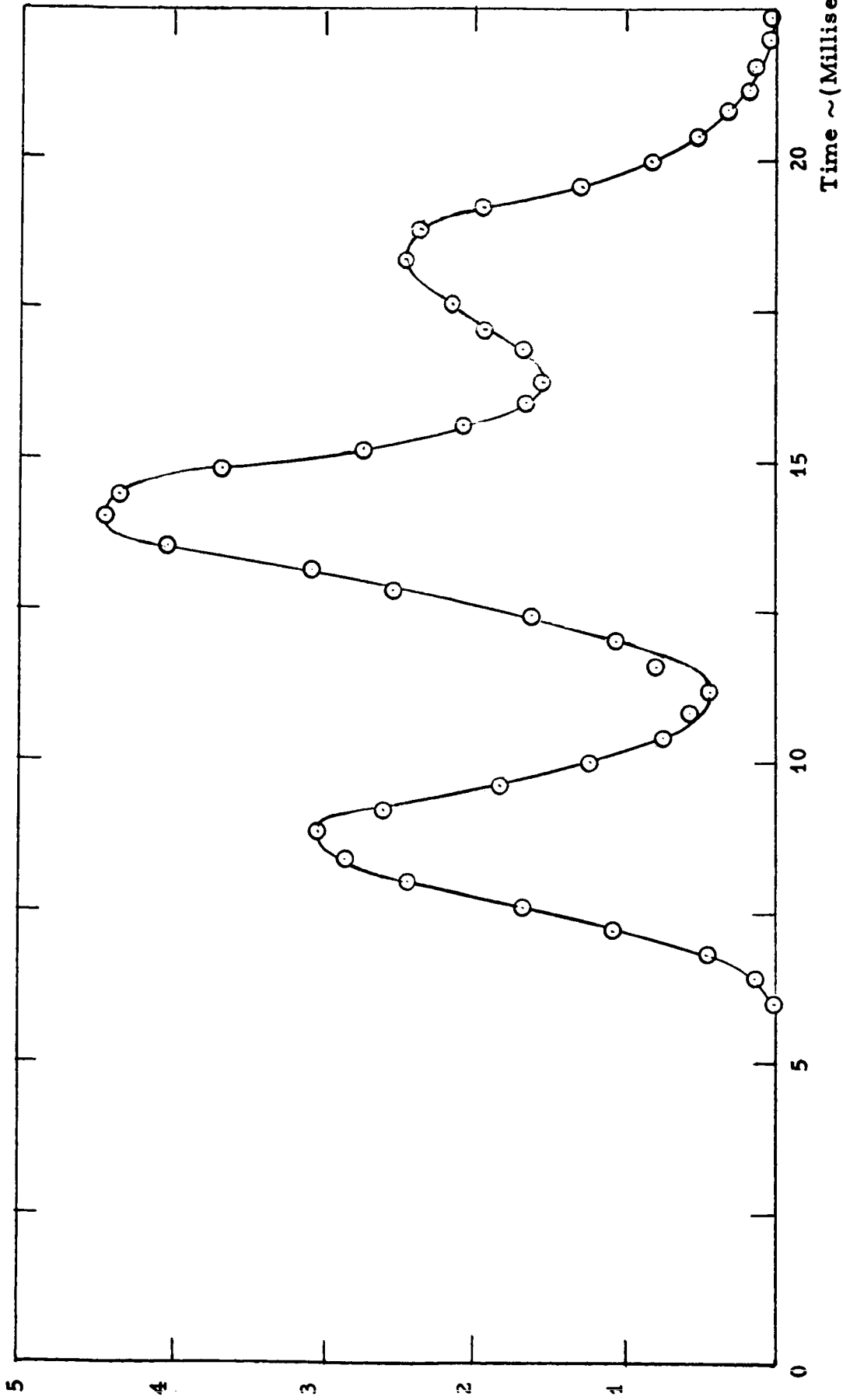


FRANKLIN GNO CORPORATION

Figure 11



Ionic Charges per Second ~  
(Particles x 10<sup>-7</sup>)



TIME DISTRIBUTION OF ALL IONIC CHARGES PER SECOND  
ARRIVING AT THE CONTROL GRID FOR ONE PHOTOPULSE  
5% C<sub>7</sub>F<sub>16</sub> IN AIR  
(Run 560)

In order to eliminate observed capacitive coupling of the anode to the control grid and the cathode, a  $10^{10}$  ohm resistor was placed in series with the anode. This resistor was located inside the electrometer and converted the apparent observed voltage source, due to capacitive coupling between the elements of the drift chamber, to a current source which is integrated effectively without overloading the instrument. The resistor was heavily shielded to reduce noise pickup. As a result of this change, operation of the electrometer is now linear down to the  $0.001 \times 10^{-10}$  ampere full scale setting. Prior to this improvement, it was demonstrated that the amplifier and the electrometer was becoming saturated on the low current scales and linear behavior was impossible.

Pickup noise and microphonics were effectively eliminated by removing the wire braid shielding over the input cable and making a direct connection to the drift chamber. In addition, a faulty input connector on the electrometer was replaced. This connector appeared to be a major source of microphonic noise and has been faulty since the instrument was first put into use.

Following the improvements outlined above, reliable data such as that reported in Figure 8 were commonplace. That is to say, the output of the electrometer is linear on the low-current scales, thus making it possible to analyze the results in terms of physical phenomena occurring within the drift chamber. We emphasize this behavior because of its obvious importance to the analysis of the data obtained throughout the research effort outlined under the contract.

#### 2-3-4-2 Experimental Observations for Typical Electrophilic Materials in Air

We have carried out electron attachment measurements for the electrophilic materials listed in Section 2-1 of this report at a variety of concentrations in dry air.

In this section of the report, we will present only typical recorder tracings as observed throughout the research effort for all of the electrophilic materials chosen. The reason for this is that as many as three different ion species have been observed for some electronegative materials at certain concentration in dry air. With this in mind, it is difficult to ascribe a definite mobility to a given electronegative material. In order to obtain a clearer understanding of the phenomena which are occurring, it is necessary to observe the entire process of electron capture as it is measured in our drift chamber apparatus. In Section 2-3-4-3 below, the total results will be summarized

for the benefit of the reader in tabular form. Following that, a discussion of attachment results will be presented, and analyses made. In Figures 13 and 14 are shown a number of recorder tracings of the electrometer current as measured at given concentrations of the various electronegative materials in dry air.

While it is possible to show all of the recorder tracings obtained under this contract, such a procedure would be not only space consuming but pointless. Suffice it to say that, at certain concentrations, some of those electronegative materials which show as many as three peaks at some concentrations, shown the presence of two or less at other concentrations. This behavior could be caused by the fact that the mobilities of two of the ion species merge, or that one ion species no longer forms at a lower concentration of the electrophilic material in the working medium.

#### 2-3-4-3 Tabulation of Attachment Results

Table II summarizes pertinent information regarding the concentration, mobility, and  $Q/Q_0$  for each of the chosen electrophilic materials in air. In cases where more than one ion peak is observed, each species is assigned a capital letter corresponding to its reduced mobility. When such a peak disappears, or merges with another peak, that letter is no longer identified with the particular ion in question.

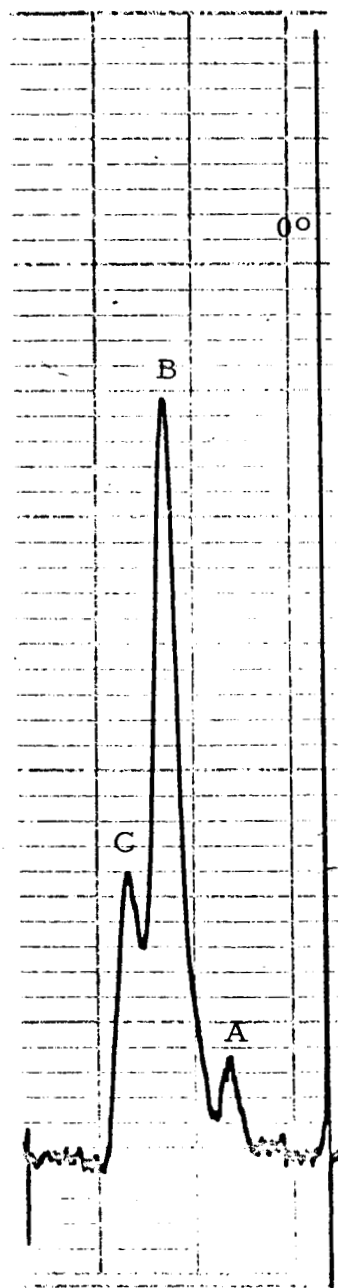
#### 2-4 Discussion and Analysis of Attachment Data

##### 2-4-1 Observed Values of $Q/Q_0$

The measured values of  $Q/Q_0$  do not appear to vary considerably from unity at any concentration of the electrophilic material in the working medium (see Table II). Even though this observation does not supply us with much comparative information between electrophilics, the lack of a pronounced deviation of  $Q/Q_0$  from unity is encouraging. It provides a positive demonstration that all of the materials tested have an exceedingly strong tendency to capture free electrons, even at low concentrations in air.

##### 2-4-2 Direct Measurement of Attachment Coefficient

It would obviously be of greater significance to parallel the above measurements by the use of a technique which would provide a comparison of the attachment coefficients of the various electrophilics. By doing so, we would have at our disposal not only ion mobilities, but also a direct comparison of other pertinent attachment characteristics.



Gas Mixture -

25.4 Torr Air

1.27 Torr  $C_6F_{14}$

$\mu_o$  Peak A -  $1.2 \pm 0.2$   $cm^2/volt\ sec.$

$\mu_o$  Peak B -  $0.8 \pm 0.1$   $cm^2/volt\ sec.$

$\mu_o$  Peak C -  $0.6 \pm 0.1$   $cm^2/volt\ sec.$



Gas Mixture -

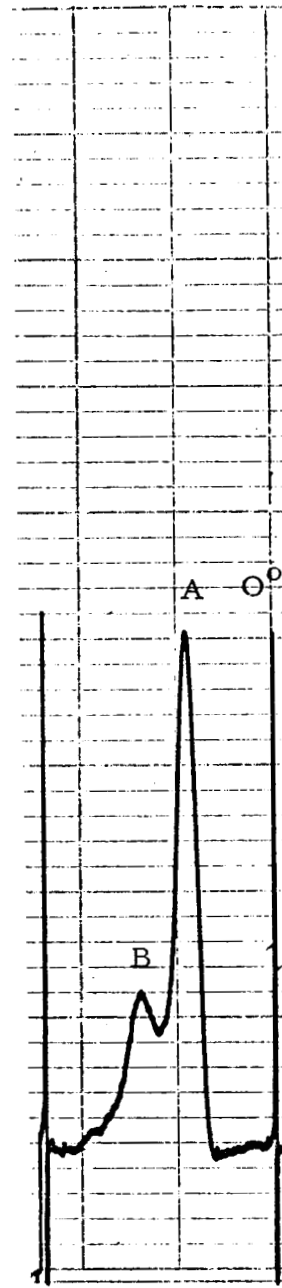
25.4 Torr Air

1.27 Torr  $C_8F_{18}$

$\mu_o$  Peak A -  $1.2 \pm 0.2$   $cm^2/volt\ sec.$

$\mu_o$  Peak B -  $0.8 \pm 0.1$   $cm^2/volt\ sec.$

$\mu_o$  Peak B -  $0.8 \pm 0.1$   $cm^2/volt\ sec.$



Gas Mixture -

25.4 Torr Air

1.27 Torr  $c-C_8F_{16}$

$\mu_o$  Peak A -  $1.3 \pm 0.2$   $cm^2/volt\ sec.$

$\mu_o$  Peak B -  $0.9 \pm 0.1$   $cm^2/volt\ sec.$

Electrometer Range -  $.003 \times 10^{-10}$  amps full scale

Motor  $t_o$  - .060 sec./rev.

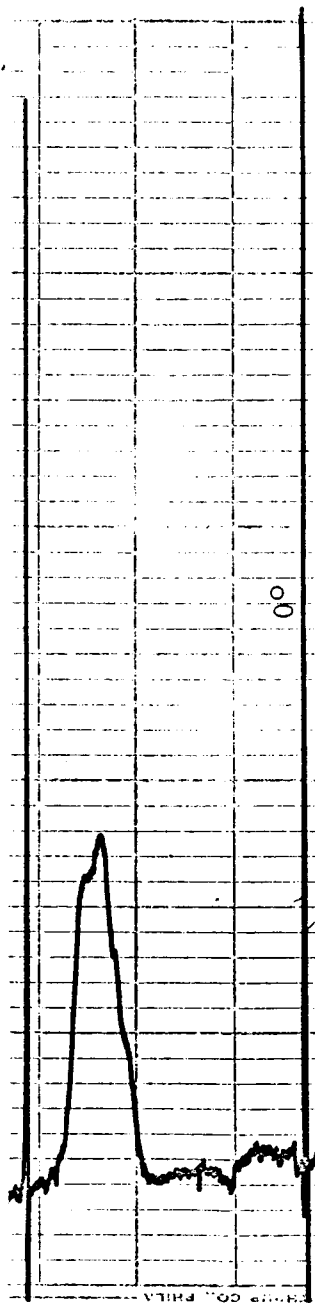
$V_{GK}$  - 130 volts

$t_g$  -  $2.0 \times 10^{-3}$  sec.

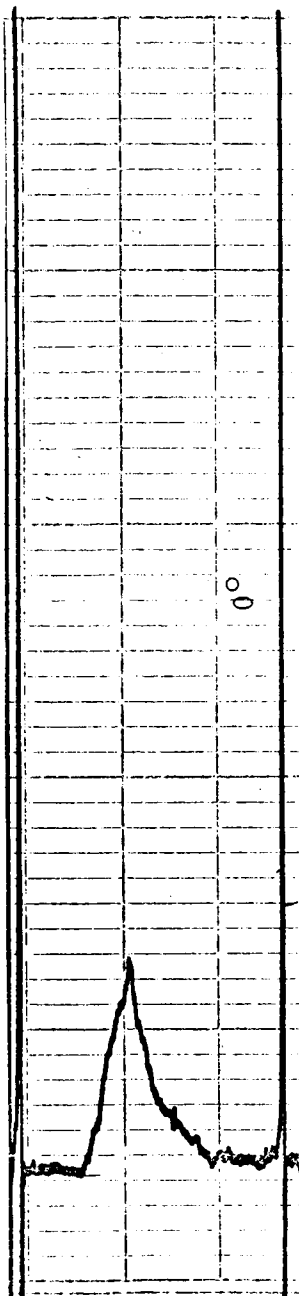


FRANKLIN GNO CORPORATION

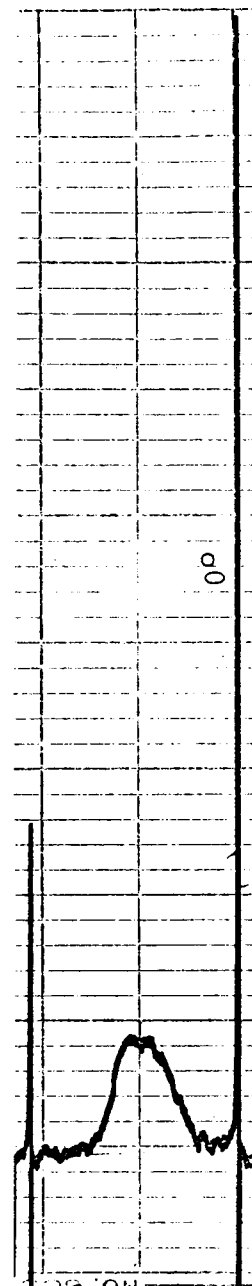
Figure 13



Gas Mixture -  
 25.4 Torr Air  
 1.27 Torr Freon E-3  
 $\mu_0 - 0.4 \pm 0.1 \text{ cm}^2/\text{volt sec.}$



Gas Mixture -  
 25.4 Torr Air  
 0.25 Torr Freon E-4  
 $\mu_0 - 0.5 \pm 0.1 \text{ cm}^2/\text{volt sec.}$



Gas Mixture -  
 25.4 Torr Air  
 0.1 Torr Freon E-5  
 $\mu_0 - 0.8 \pm 0.1 \text{ cm}^2/\text{volt sec.}$

Electrometer Range -  $.003 \times 10^{-10}$  amps full scale  
 Motor  $t_0$  - .060 sec./rev.  
 $V_{GK}$  - 190 volts  
 $t_g$  -  $3.0 \times 10^{-3}$  sec.

TABLE II  
ATTACHMENT DATA FOR MIXTURES OF  
PERFLUOROCARBONS IN AIR

Compound	Mole Fraction	E/P	$\mu_0$ (cm <sup>2</sup> /volt sec)	$i_a$ (Amps)	Q/Q <sub>0</sub>	Remarks
C <sub>6</sub> F <sub>14</sub>	0.1	0.74	(A) ---- (B) 0.65 (C) 0.53	4.7 x 10 <sup>-13</sup>	1.1	Trace of peak (A) forming; (B) is major peak
	0.05		(A) 1.22 (B) 0.75 (C) 0.61	5.5 x 10 <sup>-13</sup>	0.75	Three distinct ion peaks
	0.125		(A) 1.96 (B) 1.09 (C) ----	6.1 x 10 <sup>-13</sup>	0.96	Peak (C) merging into peak (B)
	0.003		(A) 2.62 (B) 1.31	5.8 x 10 <sup>-13</sup>	1.1	Peak (C) completely merged into peak (B)
C <sub>7</sub> F <sub>16</sub>	0.1	0.74	(A) 0.98 (B) 0.61 (C) 0.50	5.6 x 10 <sup>-13</sup>	0.97	(B) is major peak, (C) > (A)
	0.05		(A) 1.2 (B) 0.72 (C) 0.60	7.0 x 10 <sup>-13</sup>	0.94	(B) is major peak, (C) < (A)
	0.013		(A) 1.71 (B) 1.00	8.1 x 10 <sup>-13</sup>	0.91	(B) is major peak, (C) has disappeared
	0.003		(A) 2.12 (B) 1.10	7.5 x 10 <sup>-13</sup>	0.92	(A) is now major peak
C <sub>8</sub> F <sub>18</sub>	0.1	0.74	(A) 0.90 (B) 0.62	6.2 x 10 <sup>-13</sup>	0.85	(A) ≈ (B)
	0.05		(A) 1.20 (B) 0.78	7.5 x 10 <sup>-13</sup>	0.91	(A) > (B)

ATTACHMENT DATA FOR MIXTURES OF  
PERFLUOROCARBONS IN AIR (cont.)

Compound	Mole Fraction	E/P	$\mu_0$ (cm <sup>2</sup> /volt sec)	$i_a$ (Amps)	Q/Q <sub>0</sub>	Remarks
C <sub>8</sub> F <sub>18</sub> (cont.)	0.013	0.74	(A) 1.50 (B) 1.03	8.8 x 10 <sup>-13</sup>	0.98	(B) << (A)
	0.003		(A) 1.87 (B) 1.22	8.6 x 10 <sup>-13</sup>	0.82	(B) almost completely merged into (A)
c-C <sub>8</sub> F <sub>16</sub> O	0.1	0.74	(A) 1.03 (B) 0.70	6.6 x 10 <sup>-13</sup>	0.80	(A) >> (B)
	0.05		(A) 1.35 (B) 0.89	8.0 x 10 <sup>-13</sup>	1.0	(B) disappearing
	0.013		(A) 1.63 (B) 1.03	9.0 x 10 <sup>-13</sup>	1.29	
	0.003		(A) 1.80 (B) 1.19	8.5 x 10 <sup>-13</sup>	1.42	(B) almost completely merged into (A)
Freon E-3	0.1	1.08	0.30	5.0 x 10 <sup>-14</sup>	1.25	Single ion peak
	0.05		0.39	1.2 x 10 <sup>-13</sup>	1.12	"
	0.013		0.72	3.1 x 10 <sup>-13</sup>	0.86	"
	0.003		0.87	4.4 x 10 <sup>-13</sup>	1.14	"
Freon E-4	0.035	1.08	0.49	4.1 x 10 <sup>-14</sup>	0.89	Single ion peak
	0.018		0.51	1.0 x 10 <sup>-13</sup>	0.89	"
	0.004		0.67	1.3 x 10 <sup>-13</sup>	1.06	"
	0.001		0.84	----	----	"
Freon E-5	0.017	1.08	0.80	1.0 x 10 <sup>-13</sup>	0.50	Single ion peak
	0.009		0.84	6.4 x 10 <sup>-14</sup>	0.98	"
	0.0005		0.84	7.5 x 10 <sup>-14</sup>	0.94	"

It is possible to accomplish the above by resorting to the method developed by Chanin, Phelps, and Biondi<sup>3</sup>. As mentioned earlier, this differs from our technique in that the potential between cathode and control grid is maintained at a constant value throughout each experiment. The result of this is that an equilibrium distribution of electrons and negative ions is established between the two elements of the drift chamber such that a semilog plot of the current to the grid yields a linear dependence upon time during which ions are collected. The ion current follows the relationship;

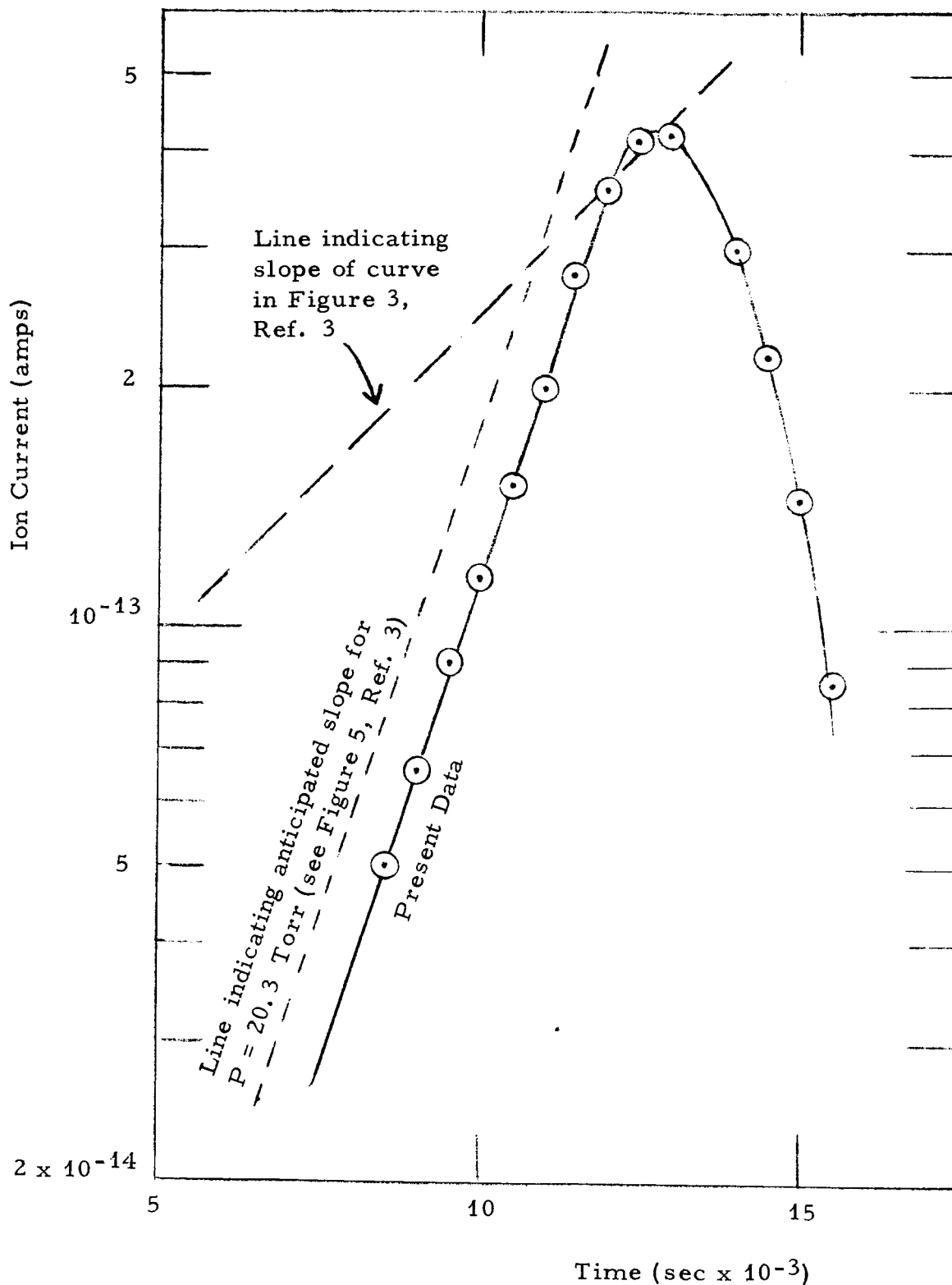
$$I(t) = I_0 \exp(\eta w_i t), \quad (2-21)$$

where  $I_0$  denotes the initial ion current reaching the control grid,  $\eta$  is the attachment coefficient per unit drift distance, and  $w_i$  is the ionic drift velocity. The value of  $\eta w_i$  is determined from the slope of the  $\ln I$  versus  $t$  plots, and  $w_i$  is evaluated from the observed transit time of the ions formed adjacent to the photocathode. This gives the numerical value for  $\eta$  under the given experimental conditions.

We have tested the above method for attachment coefficient measurements in pure  $O_2$ . The result of this effort is presented in Figure 15. Although the slope of the  $\log I$  versus  $t$  curve does not agree with that given in Figure 3 of the paper published by Chanin et al<sup>3</sup>, the latter have shown in their Figure 5 that  $\eta/P$  at low values of  $E/P$  is strongly dependent upon  $P$ . By the process of interpolation, we have estimated the slope to be anticipated at the pressure (20.3 Torr) used in our experiments. In the curve they present, the value of  $P$  was 10.5 Torr. Note the interpolated slope is within 5% of our measurements plotted in Figure 15. This observation provides a good indication that our experimental technique yields data consistent with that of the previous investigators<sup>3</sup>. Our measured value of the reduced mobility of the oxygen ion is  $2.88 \text{ cm}^2/\text{volt sec}$  which also is in close agreement with the value of  $2.7 \text{ cm}^2/\text{volt sec}$  reported by the same workers.

Although it is possible to employ the above technique directly for oxygen gas, it will not be possible to make use of it to determine the attachment coefficient of strongly electrophilic gases in the pure state. This is due to the fact that attachment is so strong that insufficient electrons can be generated by the photopulse to allow an equilibrium distribution of the latter throughout the drift distance. That is to say, essentially all of the emitted electrons will be captured long before they would normally approach the control grid.





**FN**

FRANKLIN **ENO** CORPORATION

FIGURE 15

NUMBER

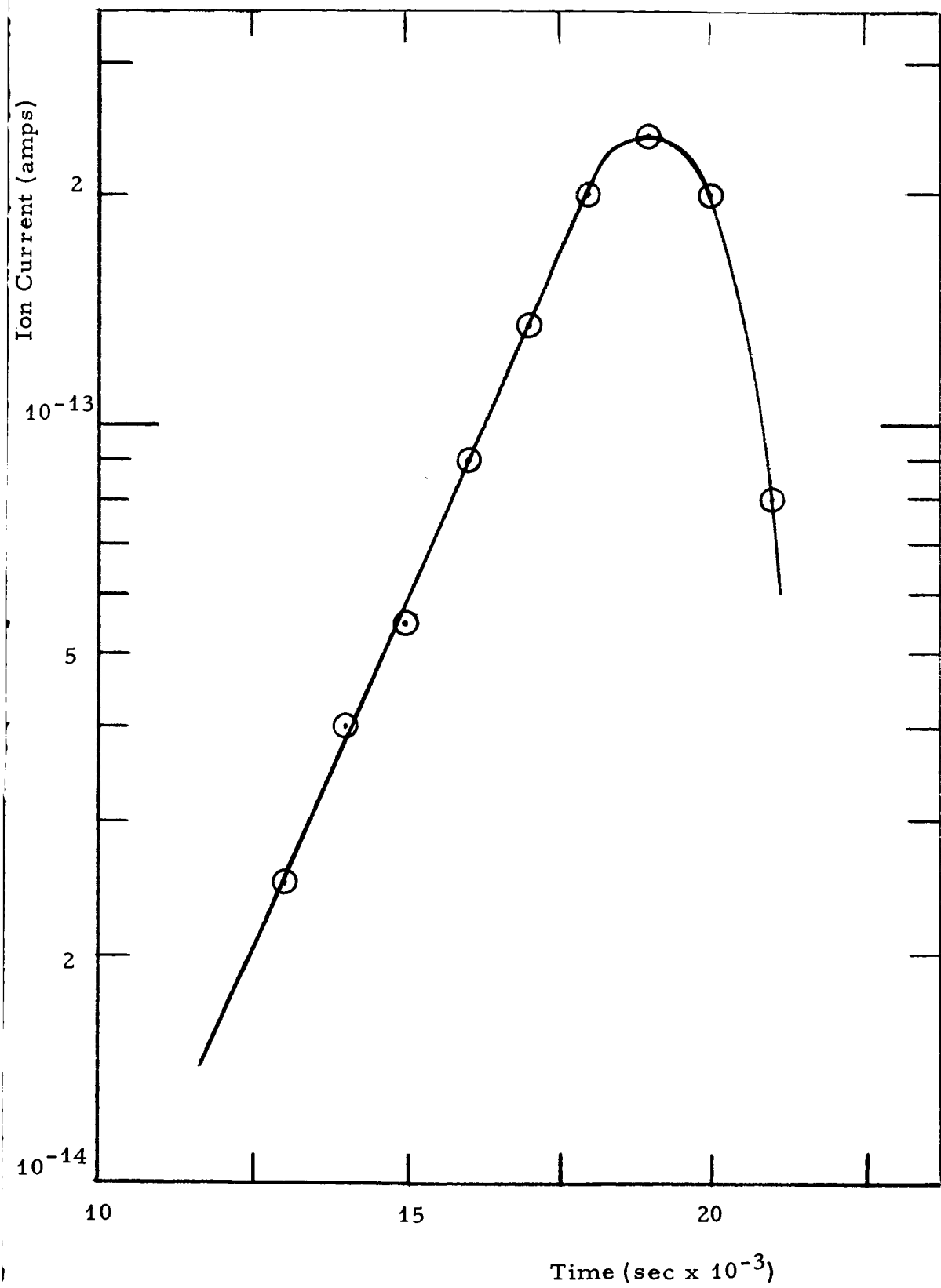
TITLE


Log I vs t  
 $O_2$  at  $E/P = 0.25$  volts/Torr cm

The technique is amenable to the quantitative investigation of "effective" attachment coefficients of electrophilics, highly diluted by inert gases such as  $N_2$  or air (see Figure 16). The results can be analyzed either by finding the concentration which yields the same value of  $\eta$ , or by comparing effective values of  $\eta$  at a given concentration. However, it is anticipated that many complicated phenomena will be associated with these measurements and their analysis. Unfortunately, time does not permit us to accomplish this before termination of the contract period.

It is possible, however, to obtain numbers from Figure 16, to show the magnitude of the value of  $\eta$  in Freon E-3 under a certain set of experimental conditions. The slope of the curve can be shown to yield a value of  $\eta w_i = 423 \text{ sec}^{-1}$ . From the known value of 374 cm/sec for  $w_i$ ,  $\eta$  is found to be  $1.13 \text{ cm}^{-1}$ . If we divide this by the pressure used (50.8 Torr), we obtain an "effective" value of  $\eta/P$  of  $0.022 \text{ cm}^{-1} \text{ Torr}^{-1}$ .

If we desire to consider only the effect of the electrophilic in the mixture, we must take into account the partial pressure of Freon E-3. Since this involves only a measurement of  $\eta$  divided by the ratio, 50.8/2900, we find an extrapolated value of  $\eta/P_i$  as high as  $64.6 \text{ cm}^{-1} \text{ Torr}^{-1}$ . This is monstrous when compared with the more common electrophilics such as  $SF_6$ . Its meaning and significance are not yet clearly understood. Further inquiry into the observation is definitely indicated.



 <b>FRANKLIN GNO CORPORATION</b>	FIGURE <i>16</i>	NUMBER
	TITLE Log I vs t Freon E-3 diluted in Air Concentration = 2900 PPM	

## SECTION III

### HIGH VOLTAGE BREAKDOWN OF ELECTROPHILIC GASES AT ELEVATED TEMPERATURES

#### 3-1 Technical Background

It is difficult to simulate re-entry because many conditions which are simultaneously important occur only during actual re-entry. Thus, even compared with other gases, the behavior of the high molecular weight electrophilics cannot be evaluated unless some basic data are available.

The purpose of the work described in this section on high-voltage breakdown is not greatly different from that described in Section II for determining the effectiveness of high molecular weight electrophilic materials to reduce electron concentration during re-entry. However, the emphasis is placed on thermal effects instead of on mobility or electron attachments at room temperatures.

High voltage breakdown in general depends on the electrophilic capability (attachment coefficient) of the gas between the electrodes. Without electrophilic capability, free electrons in the gas are accelerated by the high electric fields, and avalanches of more electrons are produced. However, when electrophilic gases are used, they act as a sponge to absorb the free electron energy, thus extending the high voltage breakdown range. This ability of electrophilic gases to affect breakdown can be exploited to examine the effectiveness of electrophilics at high gas temperatures.

The high weight molecules used here are complex and chemical decomposition (dissociation) at high temperatures is certain to alter the electron attachment properties of the parent gas. However, to preserve the total electrophilic effectiveness, the daughter products need to be only partially electrophilic, so that under certain conditions actual increase in total electron attachment per parent molecule may be possible.

The high voltage breakdown data reported here are qualitative, mostly because the method is in an early stage of development. It can be extended to temperature ranges greater than 800° K, and quantitative data can be obtained for attachment coefficients if characteristic times for avalanche formation are taken into account.

The electrophilic samples used were not diluted with air nor modified from the initial state except through reaction to the measurements. Four different gases were used: a) SF<sub>6</sub> because it has been studied extensively

and therefore represents a reference for comparing the data; b)  $C_7F_{16}$  and  $C_8F_{18}$  because they have recently become available for test purposes and represent an extension of previous work on perfluorinated hydrocarbon compounds; and  $C_8F_{16}O$  because, although the molecular weight is intermediate, the chemical structure is significantly different and may have bearing on the evaluation of the combination of electron attachment and molecular dissociation under high voltage breakdown conditions.

The high voltage breakdown data show departure from linear theory at temperatures of 700 - 800° K, but indications are that the decomposition products remain electrophilic. The results are encouraging because compared with  $SF_6$ , even the decomposition products of  $C_7F_{18}$  have more electrophilic capability.

### 3-2 Details of High Voltage Breakdown

#### 3-2-1 Avalanche and Breakdown

If there is an abrupt change in electrical resistivity between electrodes as the voltage between them is increased, an avalanche is in progress which generally results in high voltage breakdown. Since the classical experiments of Townsend<sup>7</sup>, there have been many studies of gas breakdown, and the technical literature now contains much data, discussion, and detail about this high voltage phenomena.

An ideal expression for the steady state current between electrodes under sufficient high voltage stress has been derived by Geballe and Reeves<sup>8</sup>. Not only is the avalanche effect taken into account, but also secondary effects at the cathode surface as well as the attachment coefficient are included. The general expression is:

$$i/i_0 = \frac{\left(\frac{\alpha}{\alpha - \eta}\right) e^{(\alpha - \eta)\delta} - \left(\frac{\eta}{\alpha - \eta}\right)}{1 - \left(\frac{\gamma\alpha}{\alpha - \eta}\right) \left(e^{(\alpha - \eta)\delta} - 1\right)}, \quad (3-1)$$

where  $i$  is the measured current,  $i_0$  is the initial electron current,  $\delta$  is the electrode separation (assuming a uniform field gap),  $\gamma$  is the secondary electron coefficient, and  $\alpha$  and  $\eta$  are the ionization and attachment coefficients of the gas respectively.

The general behavior for prebreakdown avalanche currents of equation (3-1) is shown in Figure 17. In this qualitative set of curves, A represents the simplest condition, with  $\gamma = 0$  and  $\eta = 0$ . Then  $i/i_0 = \exp(\alpha\delta)$ , and there is no breakdown in a strict sense because there is no voltage region where  $\lim(i/i_0) \rightarrow \infty$ . For this case, primary multiplication is the avalanche process in the gas between the electrodes.

For case B,  $\gamma \neq 0$  and  $\eta = 0$ , so that secondary effects due to cathode emission lead to a run-away current. The breakdown condition is derived from a zero denominator (equation 3-1) and occurs when  $[\exp(\alpha\delta)] - 1 = 1/\gamma$ . To predict the breakdown voltage ( $V_s$ ), it is required that the dependence of  $\alpha$  and  $\gamma$  on voltage be known.

For case C,  $\gamma \neq 0$  and  $\eta \neq 0$ , so that the effects of attachment in the gas are represented. In effect, breakdown currents are diminished by the factor  $(\alpha - \eta)$ , and the condition for breakdown is  $[\exp(\alpha - \eta)\delta] - 1 = (1/\alpha\gamma)(\alpha - \eta)$ . Note that for  $\gamma = 0$  (no surface effects), there would be no breakdown.

Case D represents a special condition where it appears possible to find a combination of values for  $\alpha$ ,  $\eta$ , and  $\gamma$  which can produce a maximum at  $\alpha = \eta$ , and a minimum at  $[1/(\alpha - \eta)] \ln[(\alpha - \eta/\gamma\alpha) + 1]$ . This case, of course, is physically real only so long as there are strong attachment forces and strong surface effects. This case has not been investigated in the present study, nor has it been reported in the literature to the best of our knowledge.

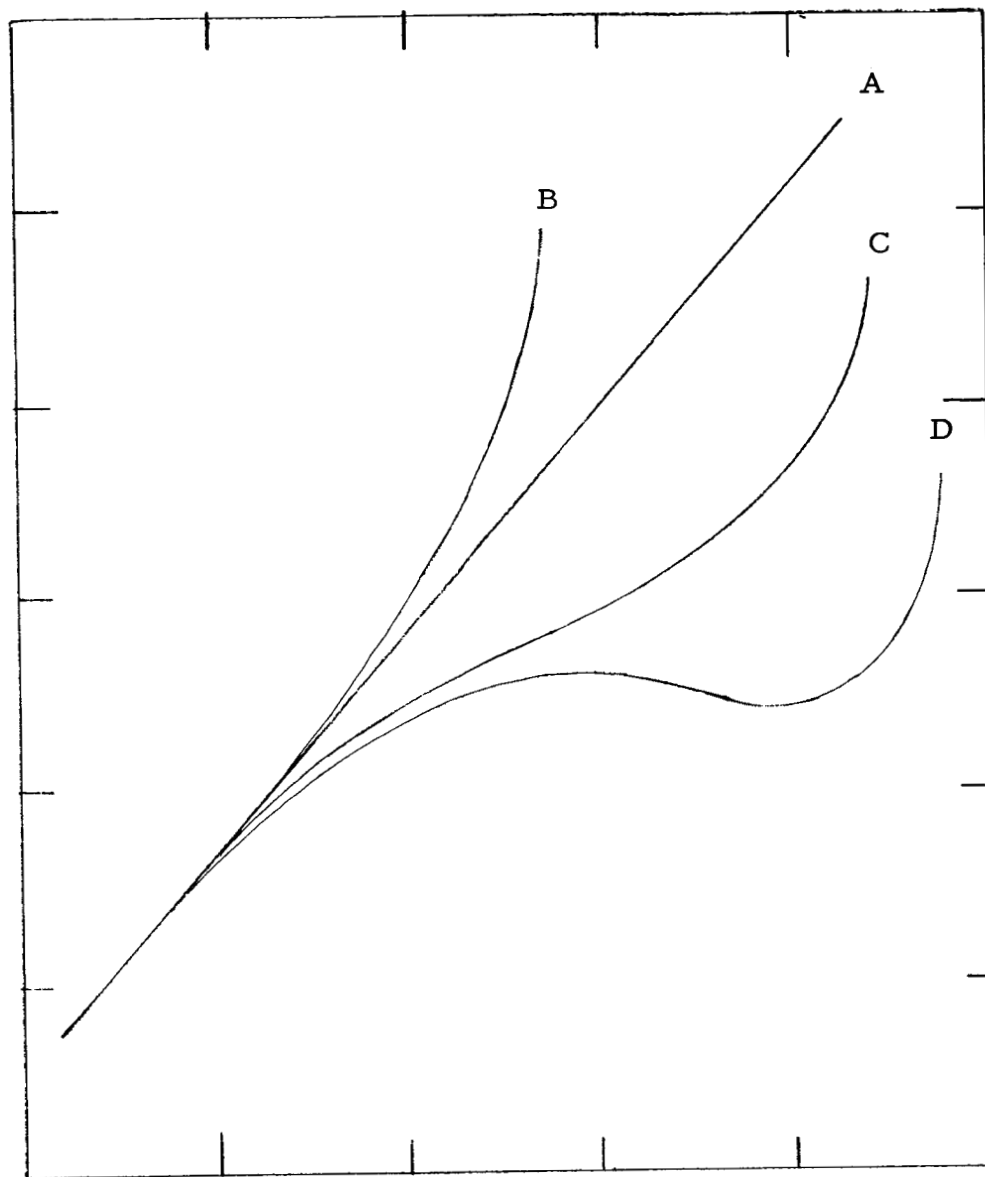
High voltage breakdown involves ionization in both time and space, but the above considerations are for steady state currents in which the number of avalanche branches are essentially limited by secondary electron mechanisms. On this account primary emphasis has been on the spatial effects associated with the interelectrode gases. Avalanche studies which involve the time for electron build-up are outside the scope of this report, but more detailed information can be found in Raether<sup>9</sup>.

### 3-2-2 High Temperature Breakdown

The high voltage breakdown between electrodes is influenced in several ways by high temperatures, but basically it is the change in chemical composition and the value of the attachment coefficient ( $\eta$ ) which is important to the present study.

To a first approximation, the high voltage breakdown ( $V_s$ ) for high pressure gases can be expressed<sup>10</sup> by the linear expression:

Prebreakdown Currents =  $\log (i/i_0) \sim$  (arbitrary units)



Gap,  $\delta \sim$  (cm)

### TYPICAL PREBREAKDOWN AVALANCHE CURRENTS

- A - Primary multiplication (Gas only)
- B - Secondary Multiplication (Surfaces included)
- C - Negative Ion Quenching (Electrophilics included)
- D - Critical Quenching

Figure 17

**FNΩ**

FRANKLIN GNO CORPORATION

$$V_s = k_1 P \delta + k_2, \quad (3-2)$$

where  $P$  is the pressure in Torr,  $\delta$  is the gap spacing in cm,  $V_s$  is in volts, and  $k_1$  and  $k_2$  are constants.

Under the assumption that the product  $P\delta$  is proportional to gas particle density between electrodes, we could write the equivalent of equation (3-2)

$$V_s = k'_1 \rho + k_2, \quad (3-3)$$

where  $k'_1$  is an appropriate new constant. For the case where the gas is at room temperature,

$$k'_1 = k_1 P_o / \rho_o. \quad (3-4)$$

Combining equation (3-4) and (3-3),

$$V_s = k_1 P_o \delta (\rho / \rho_o) + k_2. \quad (3-5)$$

For ideal gases, this is equivalent to:

$$V_s = k_1 P \delta (T_o / T) + k_2. \quad (3-6)$$

where  $T_o$  is room temperature for use with  $k_1$  also for room temperature data.

Equation (3-6) indicates that the sparking breakdown potential of a gas, including electrophilic gases, should vary directly with the ratio  $P/T$ , all other things being equal, and independent of temperature changes. According to this simplified picture, deviations from data plots  $V_s \sim P/T$  should occur only if there are changes in the gas composition.

We have made measurements of electric breakdown in  $SF_6$  for several temperatures and pressures. From the results obtained, corrections for changes in gas density due to temperature as described above were found to be necessary. However, due to the thermal expansion of the electrode support structures of stainless steel, it has also been necessary to correct for electrode separation at high temperatures. Together these corrections have been sufficient to fit existing theory well enough to distinguish non-linear effects due to gaseous decomposition in the test cell.



### 3-2-3 Thermal Stability of the Perfluorocarbons

Saturated fluorocarbons are far more stable thermally than their hydrocarbons or chlorocarbon analogues, but their stability decreases with increasing chain length or chain branching<sup>11</sup>. It is advisable to handle all fluorocarbons with great caution. Perfluorobutene, for example, is particularly dangerous since it is more toxic than phosgene; great care must be taken not to overheat fluorocarbons inadvertently in air.

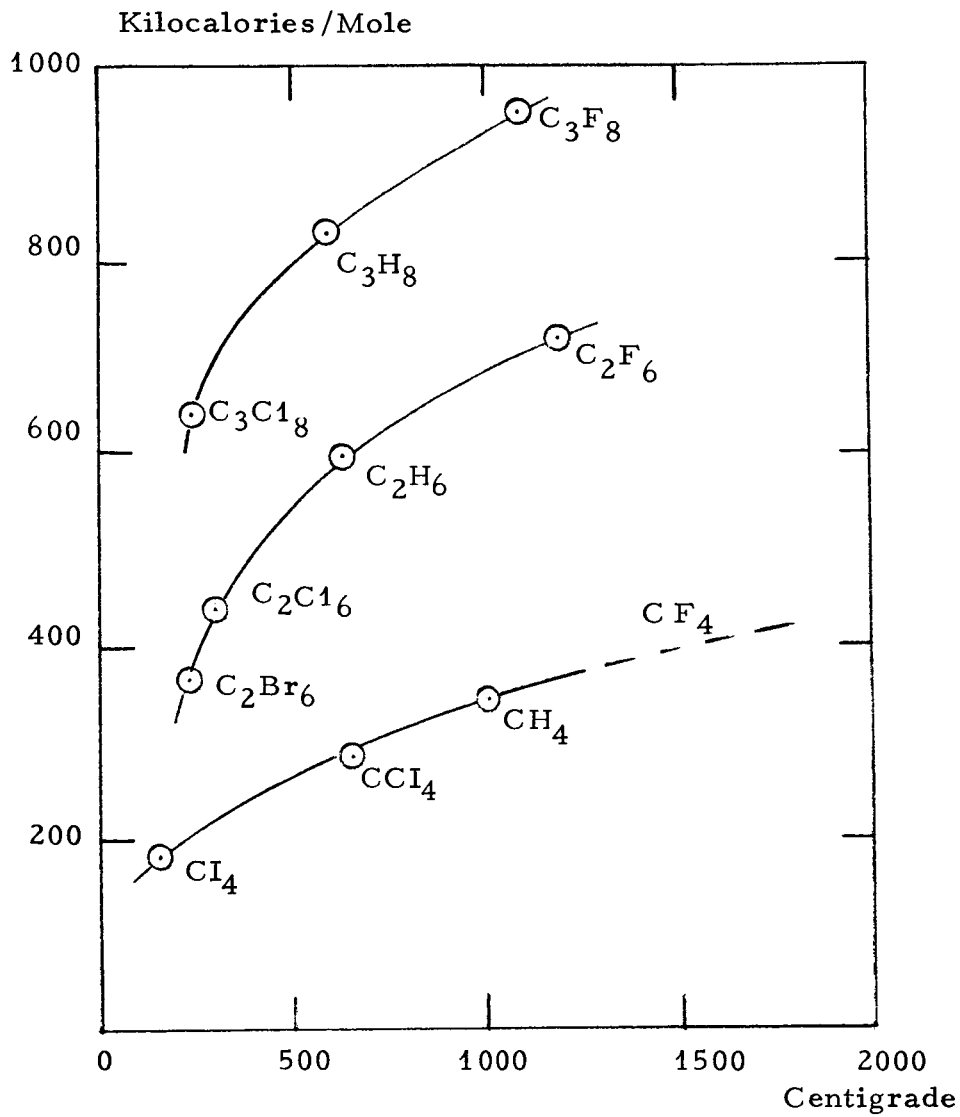
At the higher temperatures of the breakdown experiments here, it may be possible that decomposition products are a health hazard, but on the other hand there are still significant electrophilic properties to command interest in their use for re-entry plasma quenching where health is not an issue during actual use. At normal temperatures, the perfluorocarbons are among the most stable compounds known.

Figure 18 is a comparison of the thermal stabilities of a few known halogen carbon compounds. There is a trend toward lower decomposition temperatures as the molecular weights of the fluorocarbons increases. It would also be expected that greater molecular weight compounds would decompose at even lower temperatures. However, the higher molecular weight parent substances would be expected to decompose into more stable daughter compounds each with relatively high attachment probabilities.

### 3-3 Results of Experimental Breakdown

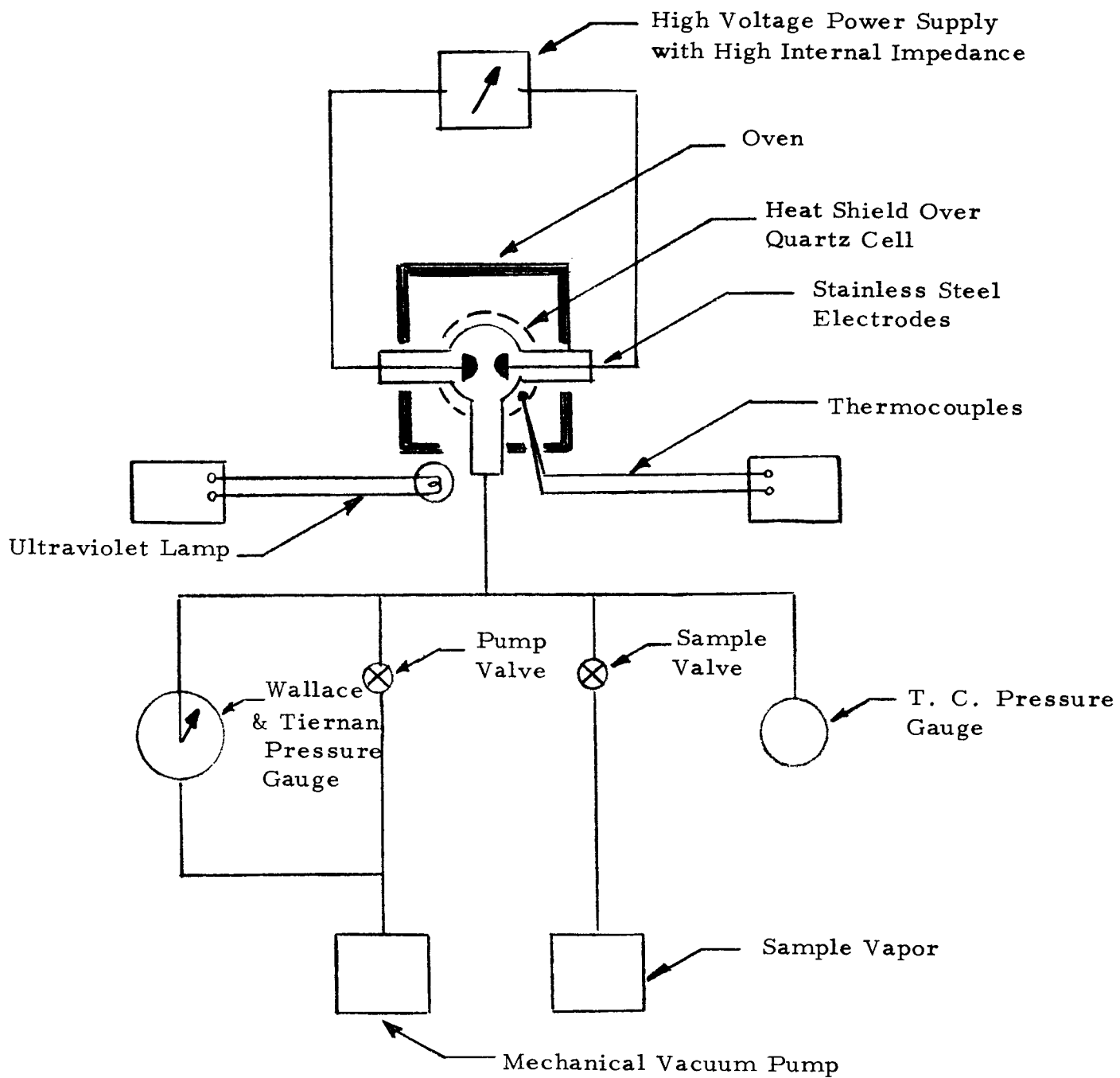
#### 3-3-1 Apparatus

A schematic of the apparatus used for the experimental data is shown in Figure 19. The quartz cell was surrounded by a heat shield to minimize thermal gradients inside the cell. A chromel-alumel thermocouple next to the glass cell was used to record the cell temperatures. Although part of the gas volume was located outside of the heat shield and outside of the oven, the location of the thermocouple accurately registered the gas temperature in the important region between the electrodes. Pressures in the gas volume were varied up to 100 Torr, and these pressures were measured with a Wallace and Tiernan mechanical pressure gauge. Vacuum valves were included in such a way that the mechanical vacuum pump could evacuate the cell, after which a second valve could be opened to admit the test gas.



COMPARISON OF THERMAL STABILITIES  
 SHOWN BY HEAT OF FORMATION FROM  
 ATOMS

FIGURE 18



HIGH VOLTAGE BREAKDOWN APPARATUS, SCHEMATIC

FIGURE 19

Electrically, a high internal impedance power supply was connected between the electrodes with a 100 megohm resistor in series to limit the breakdown current. Breakdown occurred suddenly within 1% of the applied voltage if a weak auxiliary ultraviolet lamp were used to irradiate the discharge area. The use of the uv lamp was unimportant to the accuracy of the data because it was statistically determined that similar breakdown voltages were obtainable either with or without the uv lamp. However, the spread in data from repeated breakdown trials was less with the uv lamp because of the reduced formative time lag<sup>12</sup>. Breakdown could be detected by a capacitatively coupled oscilloscope.

In operation, the voltage was increased manually and breakdown was detected either by the oscilloscope or by a drop in voltage observed on an attached voltmeter. The cell was heated in an oven at approximately 100°C intervals, about half an hour being required to establish uniform temperatures. Each gas filling was exhausted after a breakdown determination to prevent a carry-over of decomposed gases. In this way, the operation of the equipment produced reliable data.

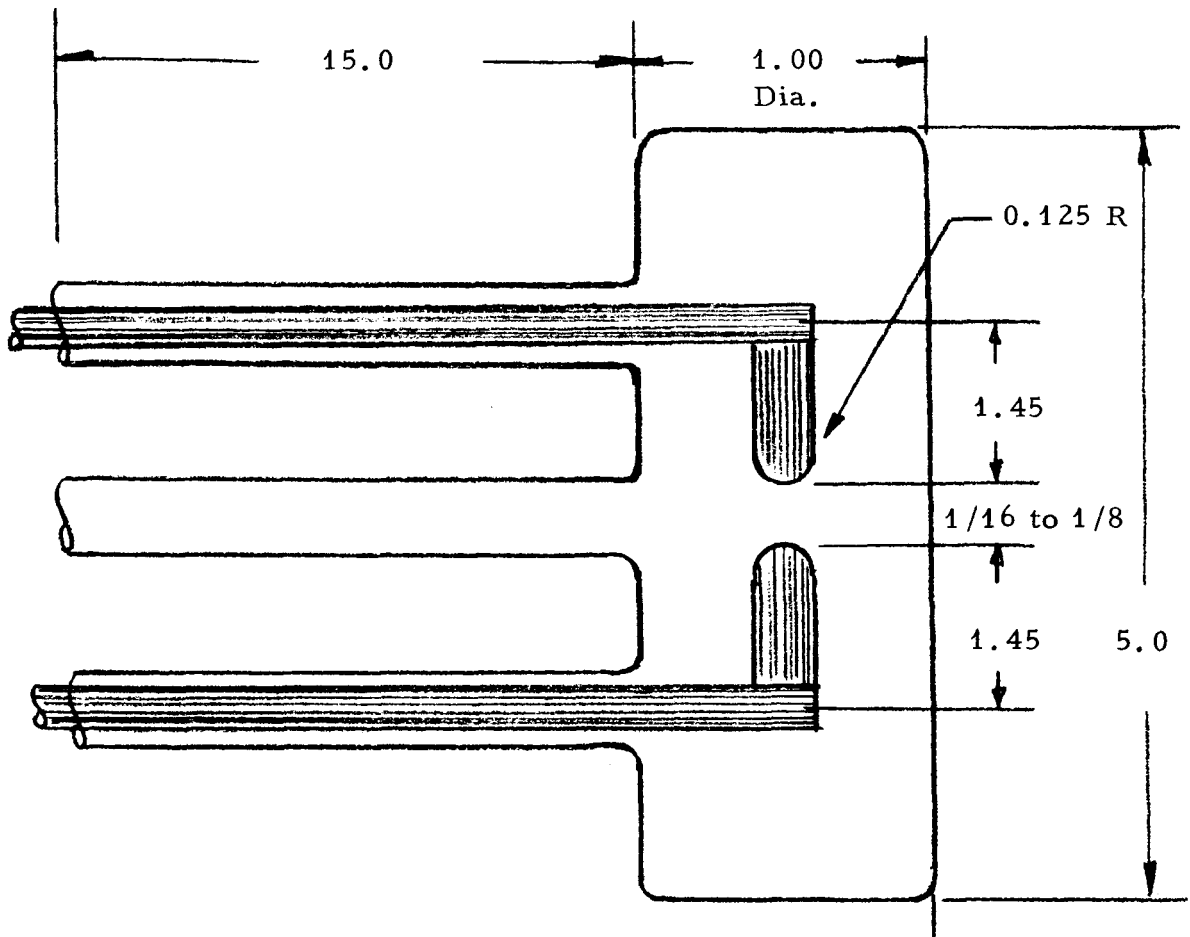
Details of the test cell are shown in Figure 20. Each of the two successful models had a different gap spacing (0.193 and 0.35 cm). The cell was quartz, and all internal metal parts were made of stainless steel which became slightly corroded as the result of high temperature and breakdown use. The gap dimensions were ascertained through comparison with known SF<sub>6</sub> data and by visual measure.

### 3-3-2 Sulfur Hexafluoride (SF<sub>6</sub>)

Data for SF<sub>6</sub> is shown in Figures 21 and 22. The gap at room temperature was 0.35 cm, and at higher temperatures, the gap reduced to 0.26 cm. The data is presented with corrections for the gap, thus normalizing breakdown values to room temperatures gap dimensions. For example, using the linear breakdown relation equation (3-2) the observed values of V and δ lead to a "corrected" value V' at δ<sub>0</sub> of:

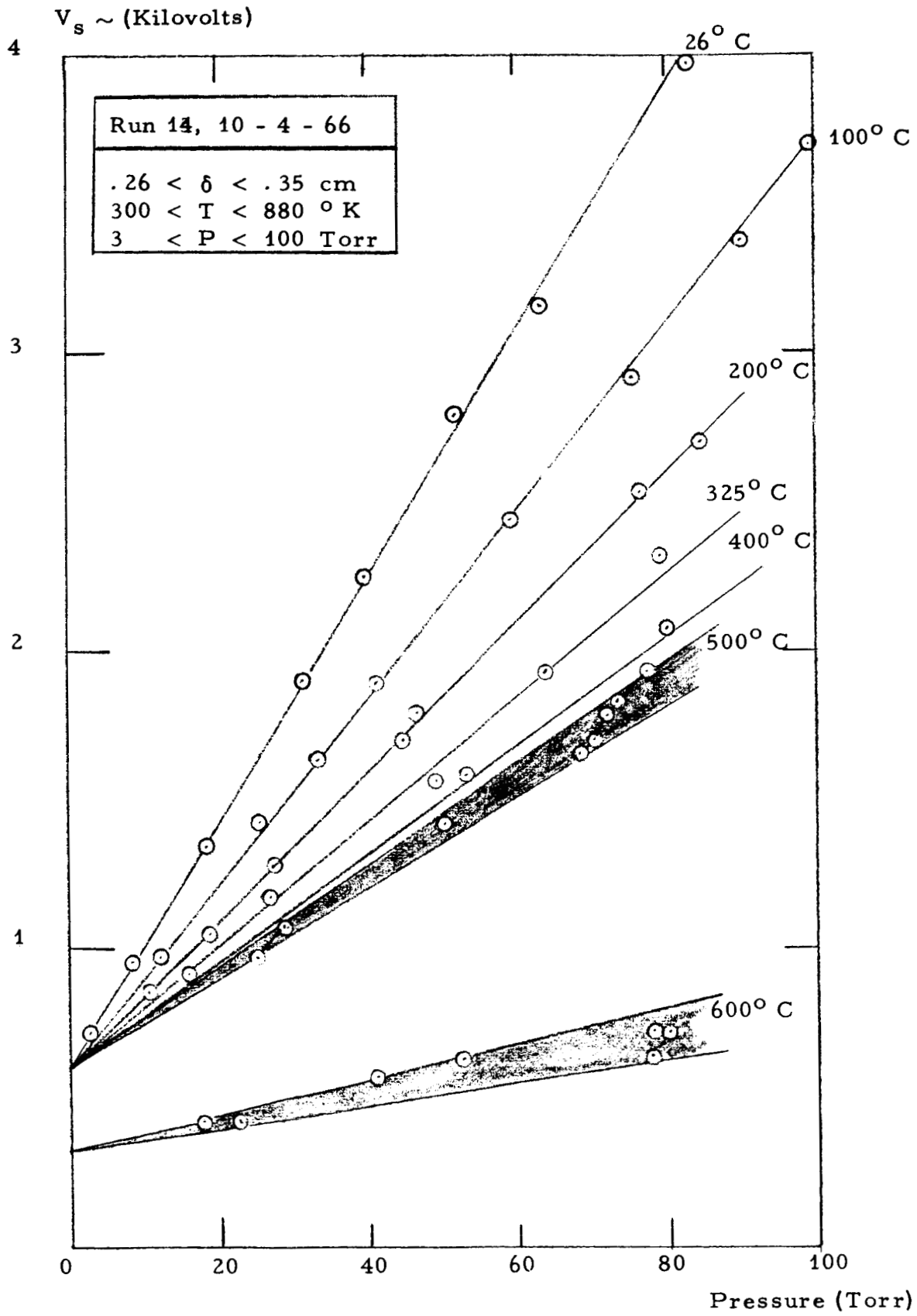
$$V' = \frac{V - k_2 (\Delta\delta / \delta_0)}{1 - (\Delta\delta / \delta_0)}, \quad \Delta\delta = \alpha (\Delta T) \quad (2 b)$$

where ΔT is the temperature difference between the electrodes and room temperature, k<sub>2</sub> is a breakdown constant of 650 volts for SF<sub>6</sub> and b = 3.62 cm is the length of each electrode.



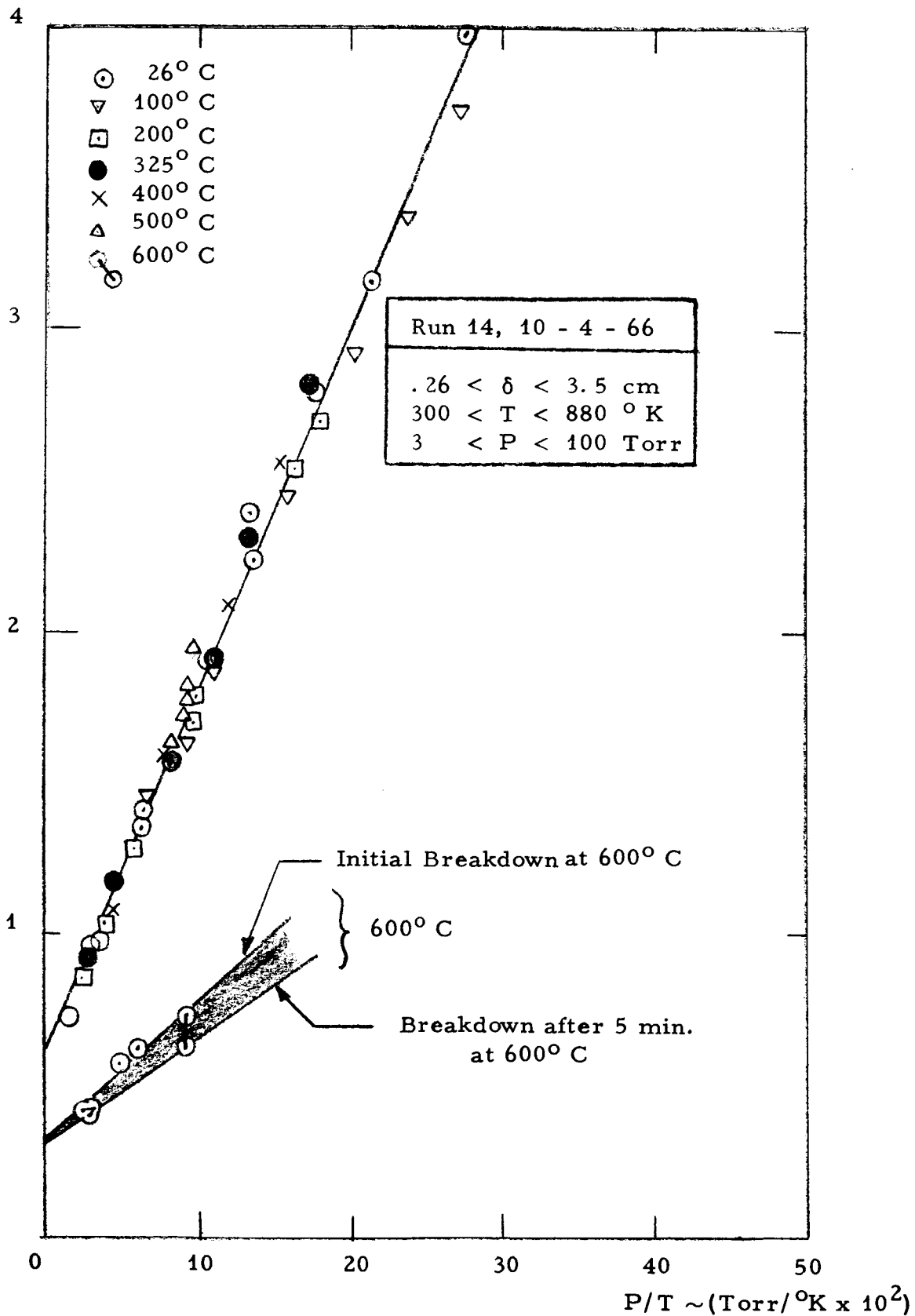
DIMENSIONS IN INCHES OF QUARTZ TEST  
CELL AND ELECTRODES

FIGURE 20



VOLTAGE BREAKDOWN CHARACTERISTIC  
FOR SF<sub>6</sub> VS T, P

$V_s \sim$  (Kilovolts)



VOLTAGE BREAKDOWN VS.  
T, P FOR SULFUR HEXAFLUORIDE ( $\text{SF}_6$ )

Note that at about 30 and 80 Torr for 500°C, there are a set of points which represent a decay in the breakdown voltage over a 5 minute period. There were no changes in the gas load during these observations. At the end of the 5 minutes, there was still a decay in pressure, but the rate of decay was less.

Data in Figure 21 is dispersed due to the different temperatures, but the variation is only a gas density change as illustrated by plotting the same breakdown vs P/T as in Figure 22. In this graph, gas decomposition in the cell shows up as clearly distinct from changes in gas density due to heating, an anticipated effect justifying the assumption that gas density is the essential variable in breakdown between the electrodes. Attachment properties apparently are much reduced for the resulting decomposition products as compared with the parent SF<sub>6</sub> gas at room temperature.

### 3-3-3 Perfluoroheptane (C<sub>7</sub>F<sub>16</sub>)

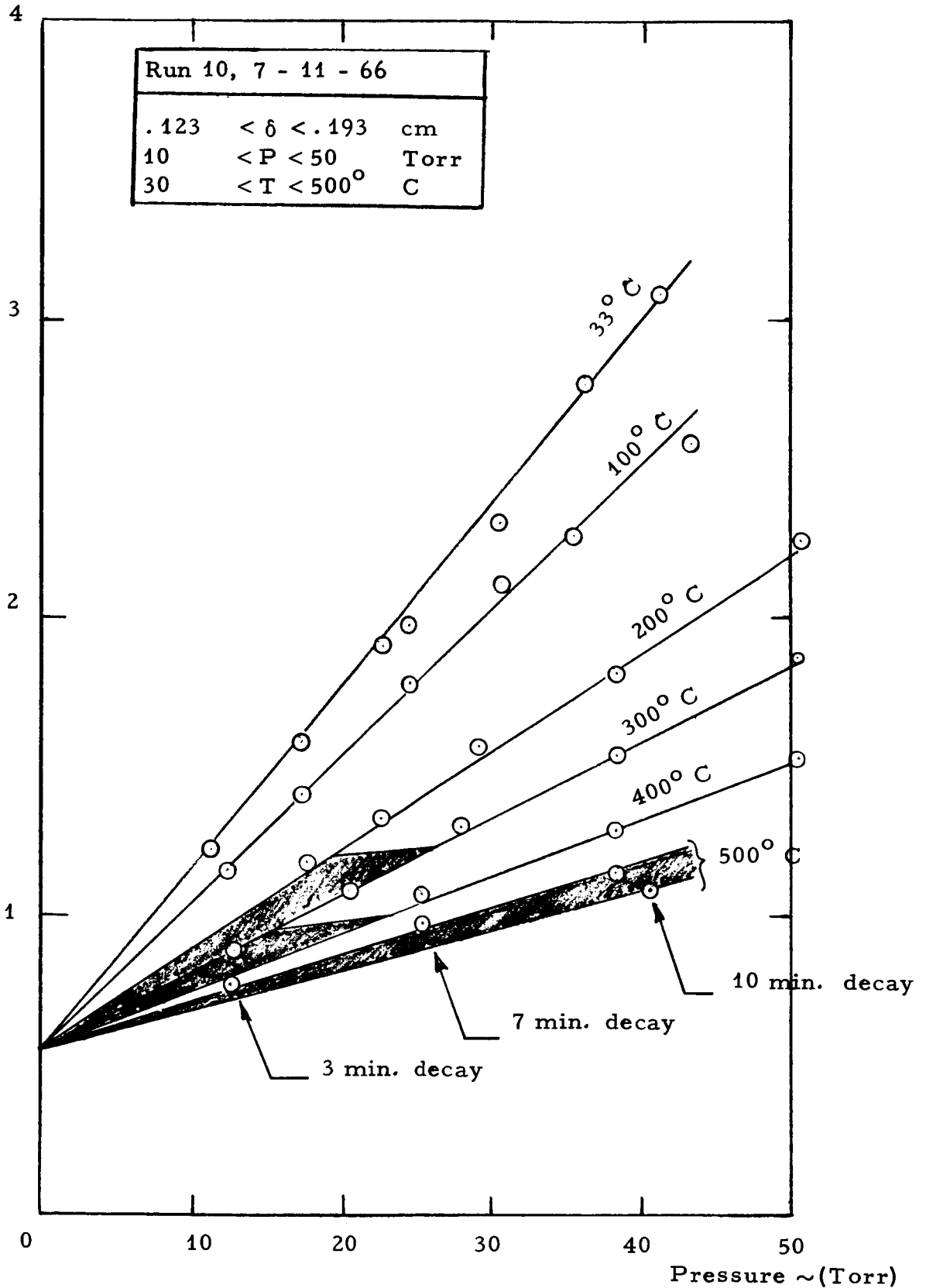
Data for C<sub>7</sub>F<sub>16</sub> is shown in Figures 23 and 24. These data were taken in essentially the same way as for SF<sub>6</sub> except the gap at room temperature was 0.193 cm which became 0.123 cm at 500°C. The constant k<sub>1</sub> (intercept of V<sub>S</sub> ~ P curve, Figure 23) is 308 volts/Torr cm, and k<sub>2</sub> = 550 volts. It is important that a) there is no detectable curvature in the V<sub>S</sub> ~ P curves for each temperature, and b) intercepts for all curves at different temperatures are identical, even with evidences of decomposition. The shaded areas indicate indeterminate regions because of pressure and breakdown changes with time (3 - 10 min.) for the same load of gas.

### 3-3-4 Perfluorooctane (C<sub>8</sub>F<sub>18</sub>)

Perfluorooctane data was taken using the same cell as for perfluoroheptane. The gap was the same (0.193 cm), and other conditions were as near similar as possible. Several initial runs were undertaken to assure that data was essentially due to the pressure of C<sub>8</sub>F<sub>18</sub>. The breakdown constants are k<sub>1</sub> = 354 volts/Torr cm, and k<sub>2</sub> = 650 volts for room temperature gas and without decomposition. Again, shaded areas in Figures 25 and 26 indicate a region of change in gas composition. The breakdown potentials exceeded those for SF<sub>6</sub> at all temperatures, indicating that the decomposition products are still relatively effective electrophilic materials.



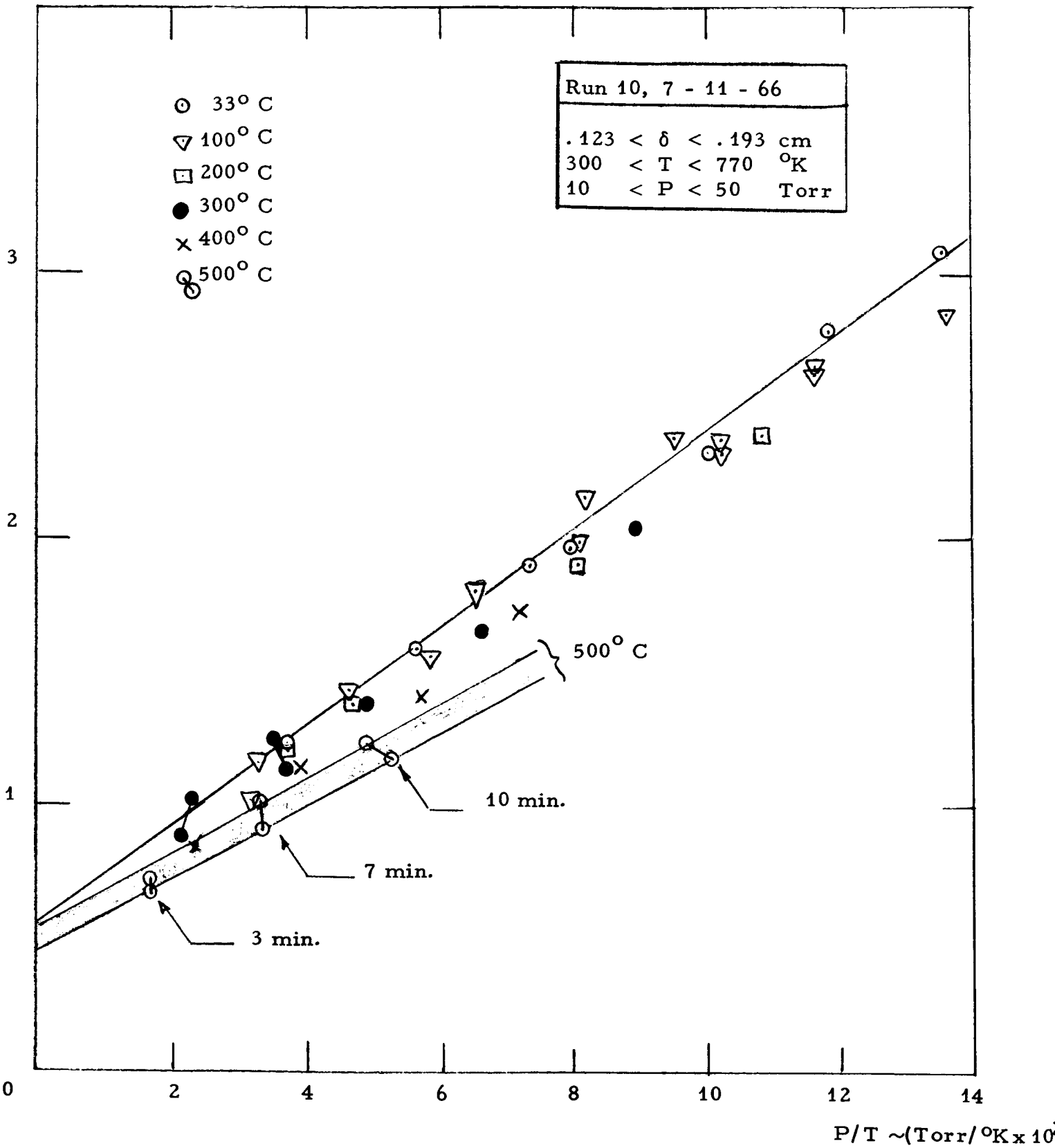
$V_s \sim$  (Kilovolts)



BREAKDOWN VOLTAGE FOR PERFLUOROHEPTANE  
( $C_7F_{16}$ ) AS A FUNCTION OF PRESSURE AND TEMPERATURE

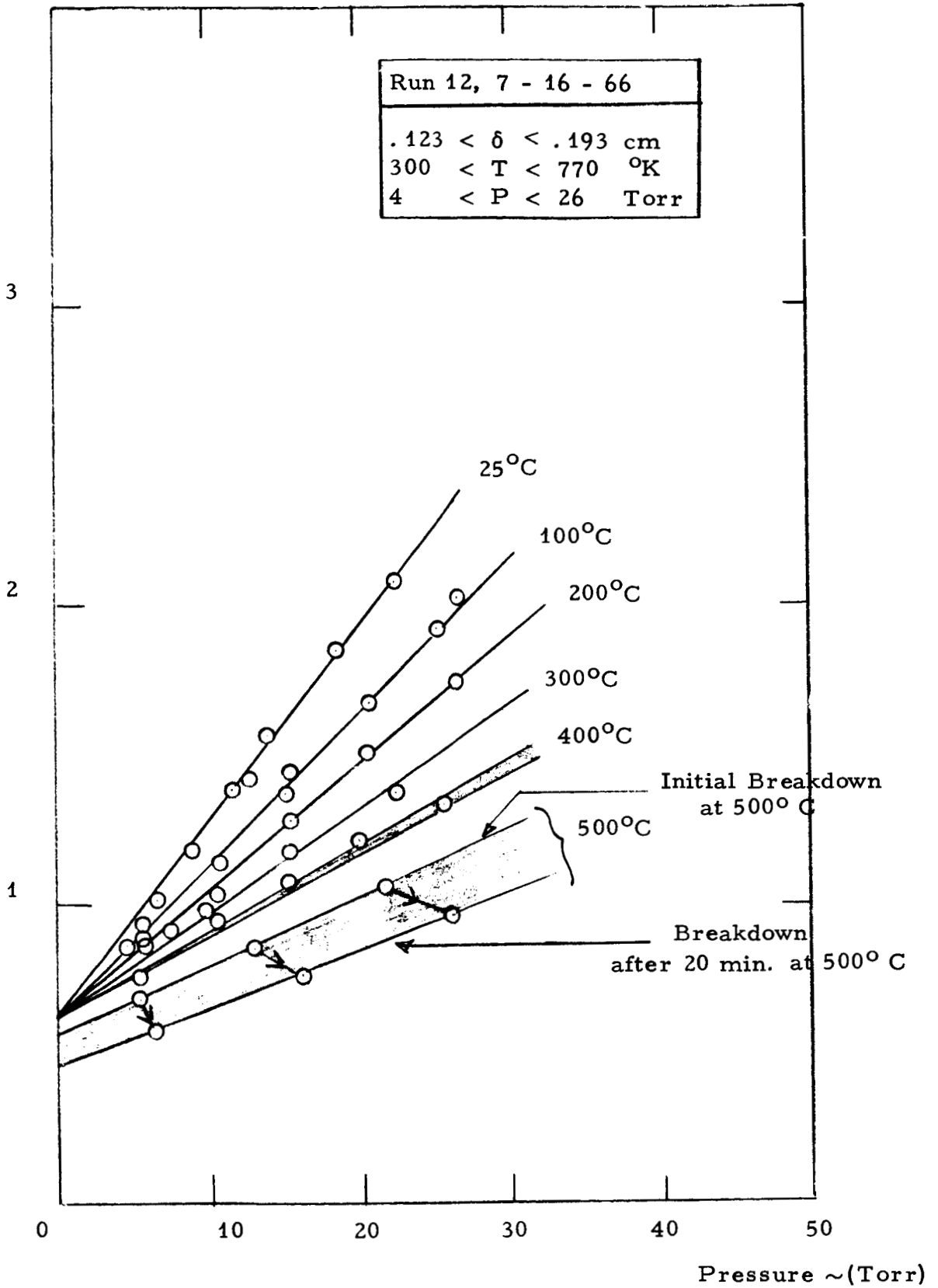


$V_s \sim$  (Kilovolts)



VOLTAGE BREAKDOWN VS. T, P FOR  
PERFLUOROHEPTANE (C<sub>7</sub>F<sub>16</sub>)

$V_s \sim$  (Kilovolts)



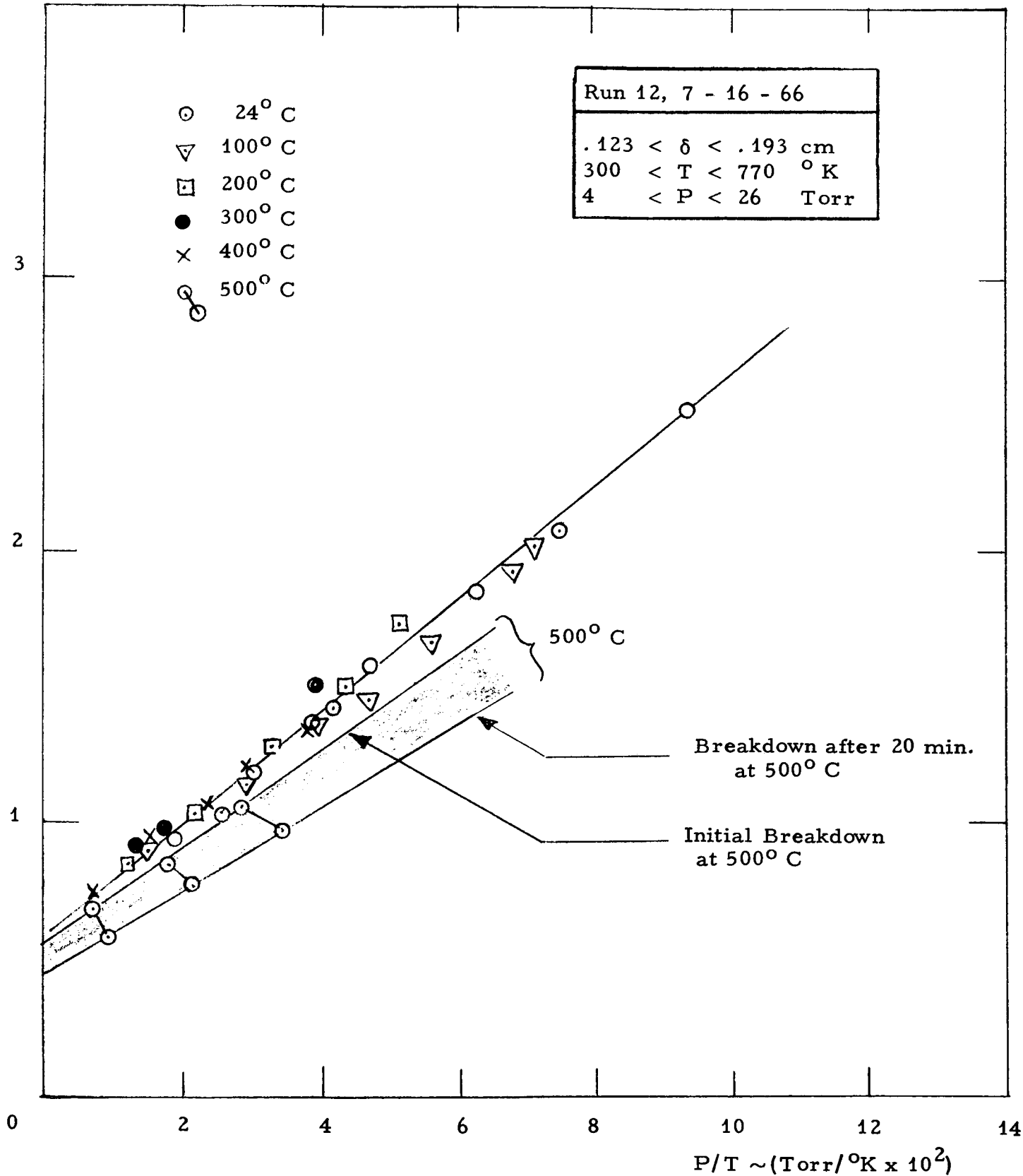
VOLTAGE BREAKDOWN CHARACTERISTIC FOR  $(C_8F_{18})$  AS A FUNCTION OF TEMPERATURE AND AND PRESSURE.



FRANKLIN OIL CORPORATION

Figure 25

$V_s \sim$  (Kilovolts)



VOLTAGE BREAKDOWN VS. T, P FOR PERFLUOROCTANE (C<sub>8</sub>F<sub>18</sub>)

Figure 26

### 3-3-5 Cyclic Perfluoroether (c-C<sub>8</sub>F<sub>16</sub> O)

Figures 27 and 28 show data for c-C<sub>8</sub>F<sub>16</sub> O as a function of pressure and temperature. In all respects, these data were taken under conditions exactly like C<sub>8</sub>F<sub>18</sub>, and the results are so similar that it is difficult to distinguish between the two materials. The breakdown constants for c-C<sub>8</sub>F<sub>16</sub> O are  $k_1 = 335$  volts/torr cm, and  $k_2 = 600$  volts.

### 3-4 Discussion of Breakdown Data

At temperatures of 700 - 800°K, there has been evidence from the high voltage breakdown that there is decomposition from the electrophilic perfluorinated gases. The resulting products, however, are apparently still electrophilic at these temperatures and more so than SF<sub>6</sub> under similar conditions. Therefore, it would be necessary to study reactions at higher temperatures if an accurate evaluation for plasma quenching during re-entry were to be made.

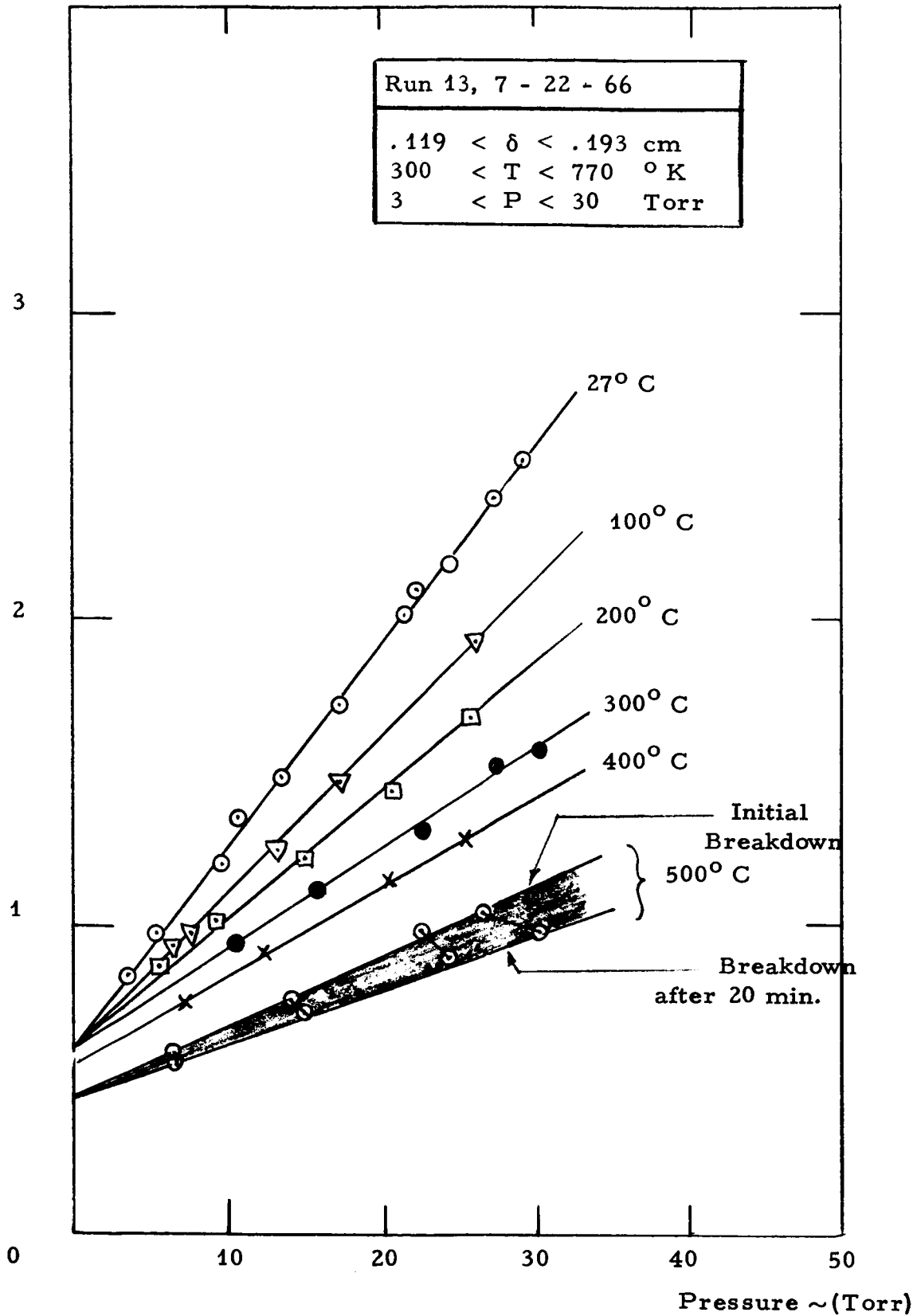
The breakdown is affected by gas density at higher temperatures, and in the course of experiment, we have determined constants for the above materials as shown in Table III. These values for SF<sub>6</sub> are in agreement with previously determined values<sup>10</sup> which lend plausibility to the values of the new materials of high molecular weight. The variation of  $k_1$  with molecular weight is an especially interesting way to compare the present data with published data for other fluorocarbons. This comparison is shown in Figure 29, in which the values of  $k_1$  are reference data.

A comparison of breakdown data for the different electrophilic gases used in these experiments at room temperature is shown in Figure 30. The similarity between C<sub>8</sub>F<sub>18</sub> and C<sub>8</sub>F<sub>16</sub>O is clearly apparent.

All conditions being equal, a graph of breakdown voltage vs  $1/T$  for constant pressure and electrode gap gives a suitable comparison between gas density and gas decomposition (see Figure 31). Near the upper temperature range of the breakdown tests, there was a gradual shift in breakdown voltage during several minutes time, as indicated by the "cross-in" lines.

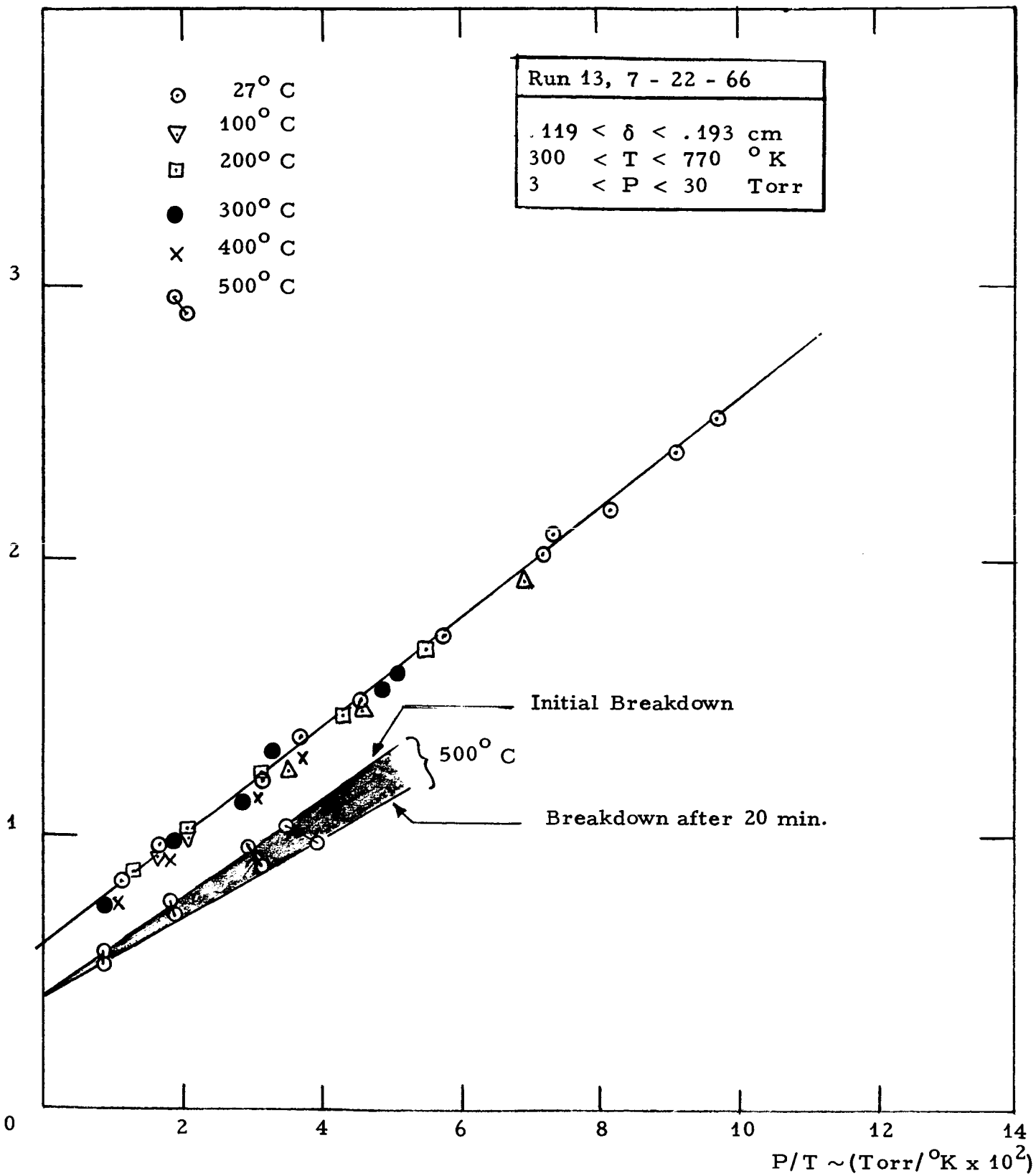
It is impossible to determine the attachment coefficients for the electrophilic gases in these experiments because, as pointed out earlier in Section 3-2-1, either  $\alpha$ ,  $\gamma$ , or avalanche buildup in time is also required to determine  $\eta$ .

$V_s \sim$  (Kilovolts)



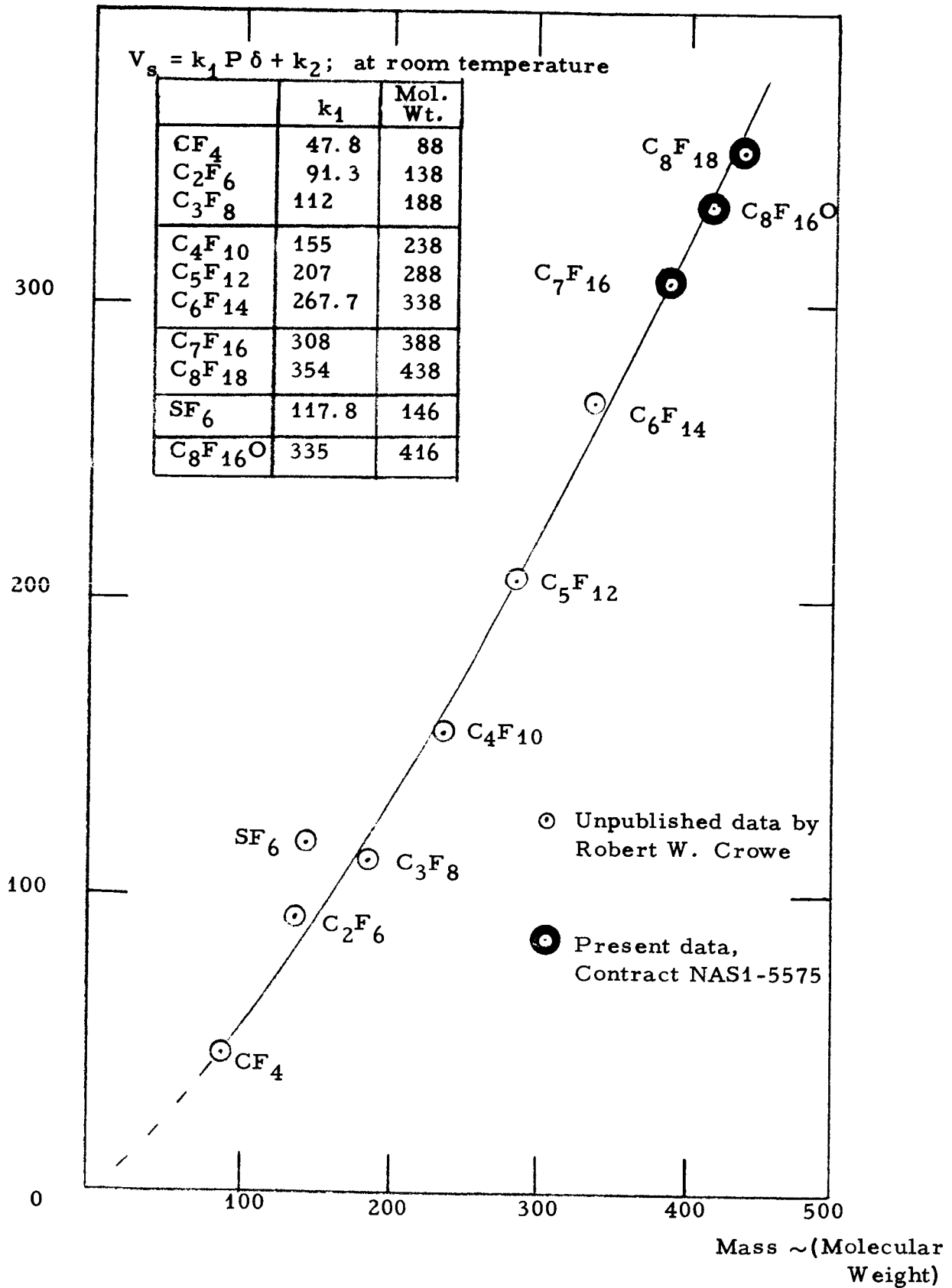
VOLTAGE BREAKDOWN CHARACTERISTIC FOR  
( $C_8F_{16}O$ ) AS A FUNCTION OF  
TEMPERATURE & PRESSURE

$V_s \sim$  (Kilovolts)



VOLTAGE BREAKDOWN VS. T, P FOR  
CYCLIC ETHER ( $C_8F_{16}O$ )

$k_1 \sim (\text{Volts/Torr} \cdot \text{cm})$

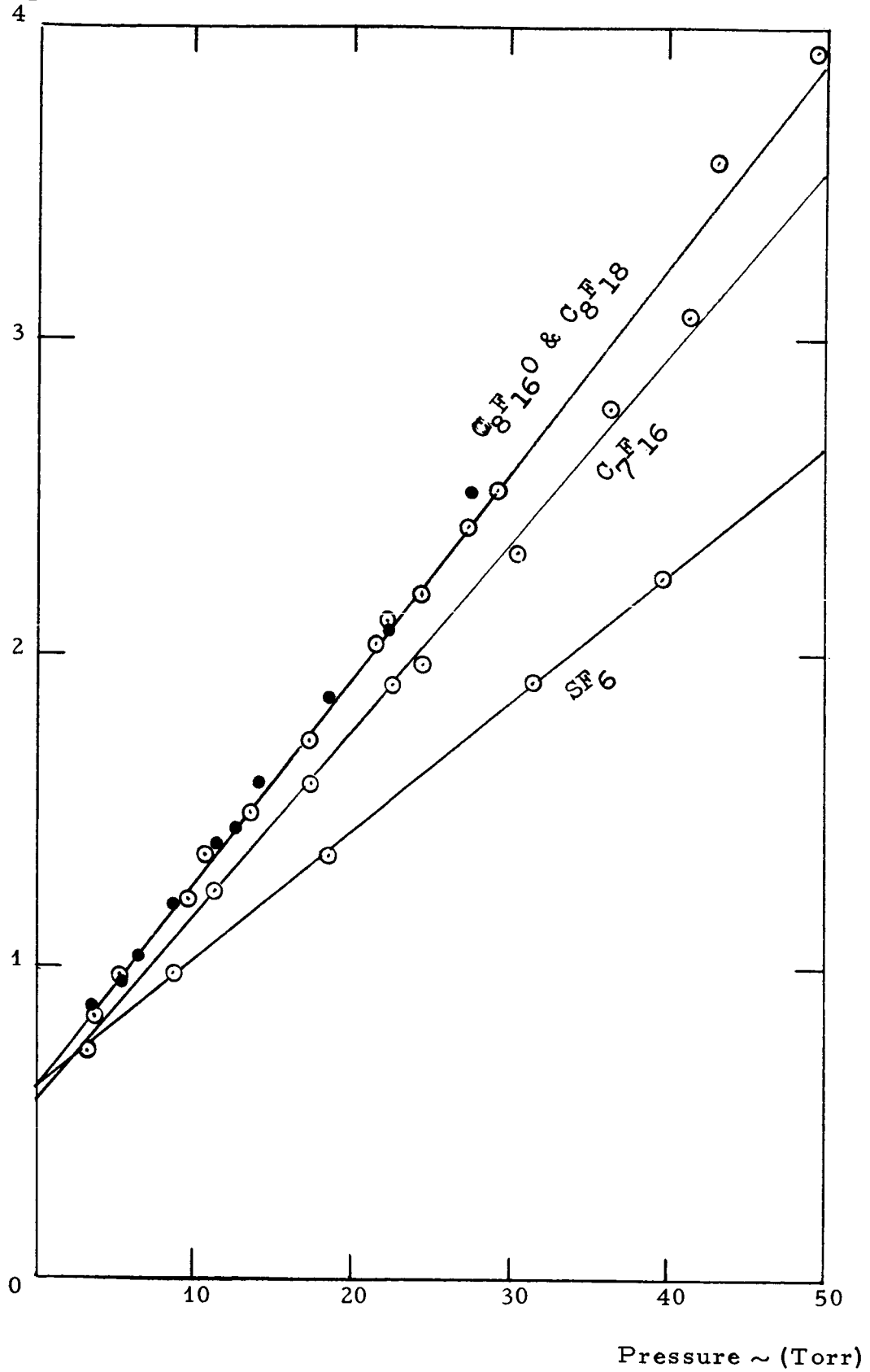


VOLTAGE BREAKDOWN CONSTANTS AT ROOM TEMPERATURE VS. MOLECULAR WEIGHT FOR FLUOROCARBONS

Figure 29

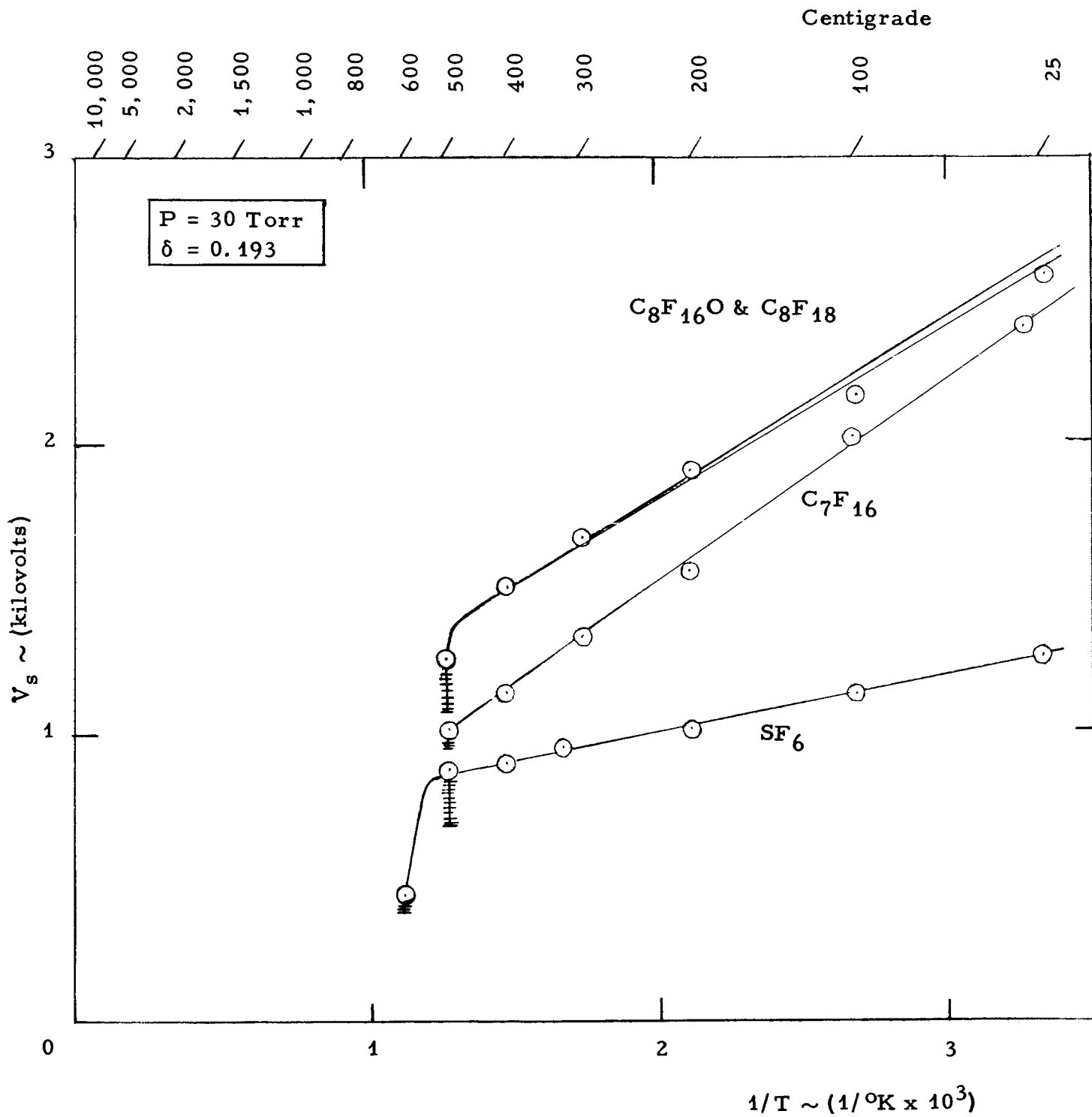


$V_s \sim$  (kilovolts)



DATA FOR BREAKDOWN AT ROOM TEMPERATURE  
FOR GAP OF .193 CM

Figure 30



TEMPERATURE VARIATION OF ELECTROPHILIC  
 BREAKDOWN WITH CONSTANT  
 $P \delta$

Wall effects in the breakdown cell may be important for decomposition, however, it was not possible to separate out the influence of such surface reactions without identifying gas components or extending the investigation to include both electrode and wall conditions.

TABLE III

BREAKDOWN CONSTANTS FOR THE  
RELATION  $V_s \sim k_1 P^{\delta} + k_2$

	$k_1$	$k_2$	Mol Wt.
S F <sub>6</sub>	117	600	146
C <sub>7</sub> F <sub>16</sub>	308	550	388
C <sub>8</sub> F <sub>18</sub>	354	650	438
C <sub>8</sub> F <sub>18</sub> <sup>0</sup>	335	600	416

## SECTION IV

### CALCULATION OF EQUILIBRIUM QUENCHING

Let us make an approximate analysis of plasma quenching in the equilibrium case, by the use of room temperature data. We will assume that instantaneous mixing of the electrophilic with the plasma occurs. Furthermore, the conditions are that the electron concentration is  $(\rho_e)_0 = 10^{13}/\text{cm}^3$  at  $t = 0$ , and must be reduced to  $\rho_e = 10^9/\text{cm}^3$  at a later time, to achieve effective quenching. Although we realize that the results obtained may have little application at elevated temperatures, it is desirable to have basic data with which to work before proceeding to more complicated situations.

Now, let us consider  $1 \text{ cm}^3$  of the plasma into which we inject a known quantity  $(\rho_M)_0$  of an electrophilic. The influence of the latter will be to reduce the concentration of electrons by converting them into negative ions. The extent of this reduction will, of course, be determined by the attachment characteristics of the electrophilic.

It is clear that the rate of removal of electrons will be governed by the expression:

$$d\rho_e / dt = \beta \rho_e \rho_M, \quad (4-1)$$

where  $\rho_e$  and  $\rho_M$  are the electron and electrophilic concentrations, respectively, at any time  $t$ . The coefficient  $\beta$  is in units of  $\text{cm}^3$  per sec. per attachment. As such, it is the product of the random velocity of the electron and the cross section of the electrophilic molecule for electron capture. Prior to determining its numerical value, let us first take another look at equation (4-1).

The solution of equation (4-1) is not difficult to obtain. It relies upon a knowledge of the functional dependence of  $\rho_e$  and  $\rho_M$  upon time. If we make the highly simplified assumption that  $\rho_e = \rho_M$ , equation (4-1) reduces to:

$$d\rho_e / dt = \beta \rho_e^2. \quad (4-2)$$

The solution of equation (4-2) is, of course,

$$\rho_e = (\rho_e)_o / [1 + (\rho_e)_o \beta t], \quad (4-3)$$

or

$$t = (1/\beta) [1/\rho_e - 1/(\rho_e)_o]. \quad (4-4)$$

Since we have already assigned a value of  $10^{13}/\text{cm}^3$  for  $(\rho_e)_o$ , the time required to reduce it to  $10^9/\text{cm}^3$  is given by

$$\begin{aligned} t &= 10^{-9}/\beta \\ \beta t &= 10^{-9} \end{aligned} \quad (4-5)$$

Now the molecular concentration can be shown by the expression;

$$\rho_M = (\rho_e)_o (K-1) + \rho_e, \quad K = (\rho_M)_o / (\rho_e)_o. \quad (4-6)$$

We then substitute equation (4-6) into equation (4-1) to obtain

$$d\rho_e / dt = \beta(K-1) (\rho_e - \beta\rho_e^2). \quad (4-7)$$

In order to simplify the above expression, we will let

$$B = \beta(K-1) (\rho_e)_o, \quad (4-8)$$

so that

$$-\int_{(\rho_e)_o}^{\rho_e} d\rho_e / (B\rho_e + \beta\rho_e^2) = t. \quad (4-9)$$

Integration yields

$$t = (1/B) \ln \left\{ \left[ \frac{B + \beta\rho_e}{B + \beta(\rho_e)_o} \right] \left[ \frac{(\rho_e)_o}{\rho_e} \right] \right\} \quad (4-10)$$

or

$$\beta t = \left[ 1 / (K-1) (\rho_e)_0 \right] \ln \left[ (K-1) (\rho_e)_0 + \rho_e \right] / K \rho_e. \quad (4-11)$$

Equation (4-11) is a general one and, as such, is applicable to situations in which gases with different numerical values of  $\beta$  are exposed to a unit volume with an initial static electron concentration  $(\rho_e)_0$ . The problem is now reduced to determination of  $\beta t$  as a function of  $\rho_e$  for assigned values of  $K$ . A family of curves showing the dependence of  $\beta t$  upon  $\rho_e$  for a range of numerical values of  $K$ , with the initially assigned  $(\rho_e)_0$ , should provide a set of results which are valid for all electrophilic materials. An accurate choice of the value of  $\beta$  renders the curves specific for the electrophilic with that value of  $\beta$ . Thus, we have the desired information regarding the influence of  $t$  and  $(\rho_M)_0$  upon  $\rho_e$ .

We have stipulated at the onset that  $(\rho_e)_0 = 10^{13} / \text{cm}^3$ , and that it was our intent to introduce electrophilic material of sufficient quantity to reduce  $\rho_e$  to  $10^9 / \text{cm}^3$ . Furthermore, it is of interest to calculate the time dependency of  $\rho_e$  reduction for various values of  $(\rho_M)_0$ . In Figure 32, we have plotted  $\beta t$  versus  $\rho_e$  for various values of  $K = 10^{-13} (\rho_M)_0$ , with the above boundary conditions taken into consideration. Note the marked, and almost consistent, decrease in  $\beta t$  with corresponding increases in  $K$ . The final step in the analysis is to introduce physically significant values of the attachment parameter  $\beta$  and to note its influence upon  $(\rho_M)_0$  and  $t$  to reduce  $\rho_e$  to  $10^9 / \text{cm}^3$ .

The definition of  $\beta$  is the product of the cross section for capture and the mean velocity of the electron. The latter is given by

$$v_e = 5.93 \times 10^7 (E)^{1/2} \text{ cm/sec.}, \quad (4-12)$$

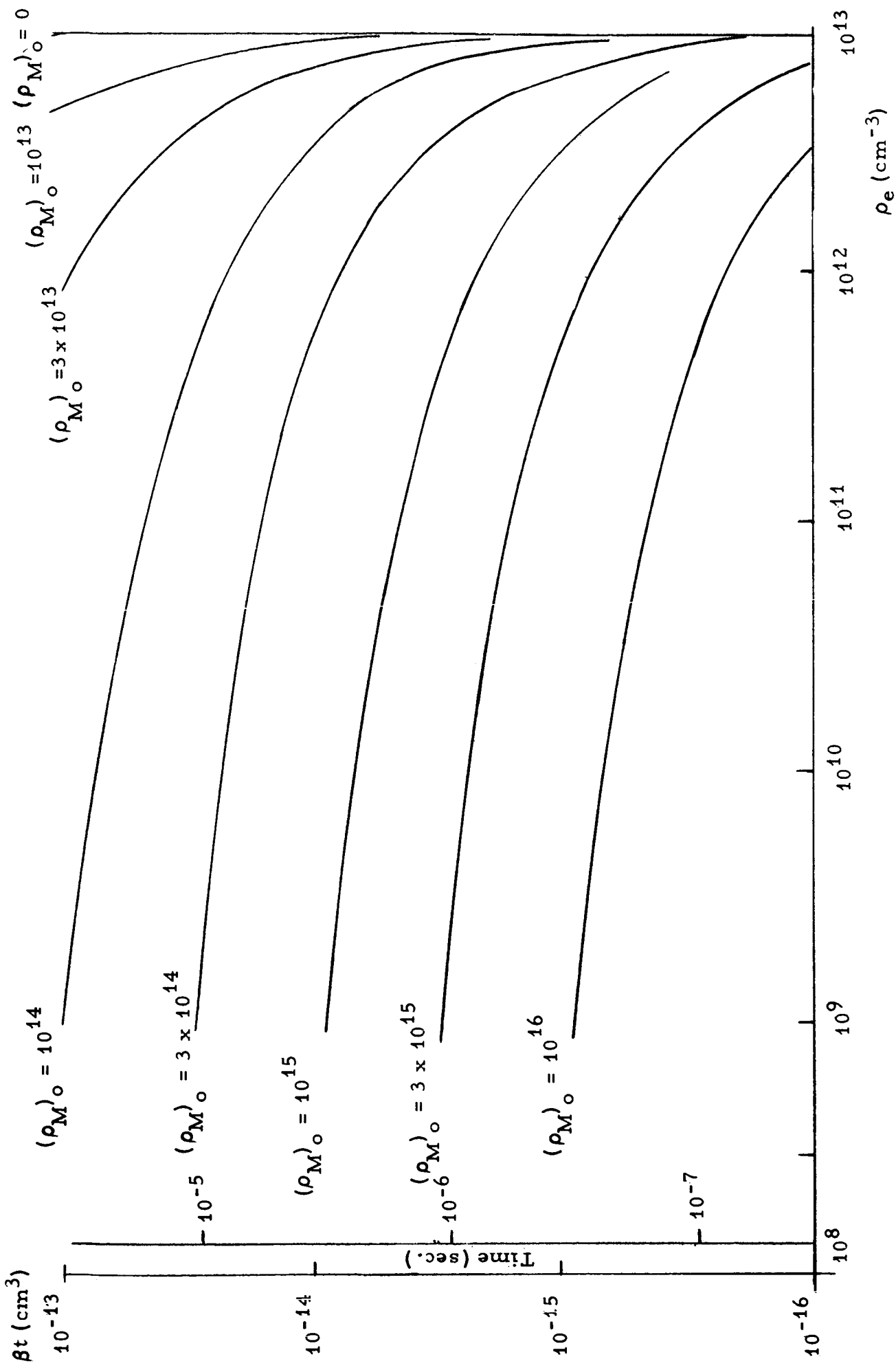
where  $E$  is the electron energy in electron volts. At a temperature of  $\sim 3000^\circ \text{K}$ ,  $E \approx 0.25 \text{ ev.}$  so that  $v_e \approx 3 \times 10^7 \text{ cm/sec.}$  It has been found that the cross section for electron capture by  $\text{SF}_6$  molecules  $\sigma_A$  is of the order of  $10^{-16} \text{ cm}^2/\text{molecule}$ .<sup>6</sup> Therefore

$$\beta = v_e \sigma_A \approx 3 \times 10^{-9} \text{ cm}^3/\text{sec.} \quad (4-13)$$

Another way of presenting the information in equation (4-11) is to calculate  $K$  versus  $\beta t$  for selected values of  $\rho_e$  from  $10^{13} / \text{cm}^3$  to  $10^9 / \text{cm}^3$ . This would show the relationship between  $(\rho_M)_0$ , time, and the desired final value of  $\rho_e$ . Such a family of curves is plotted in Figure 33.

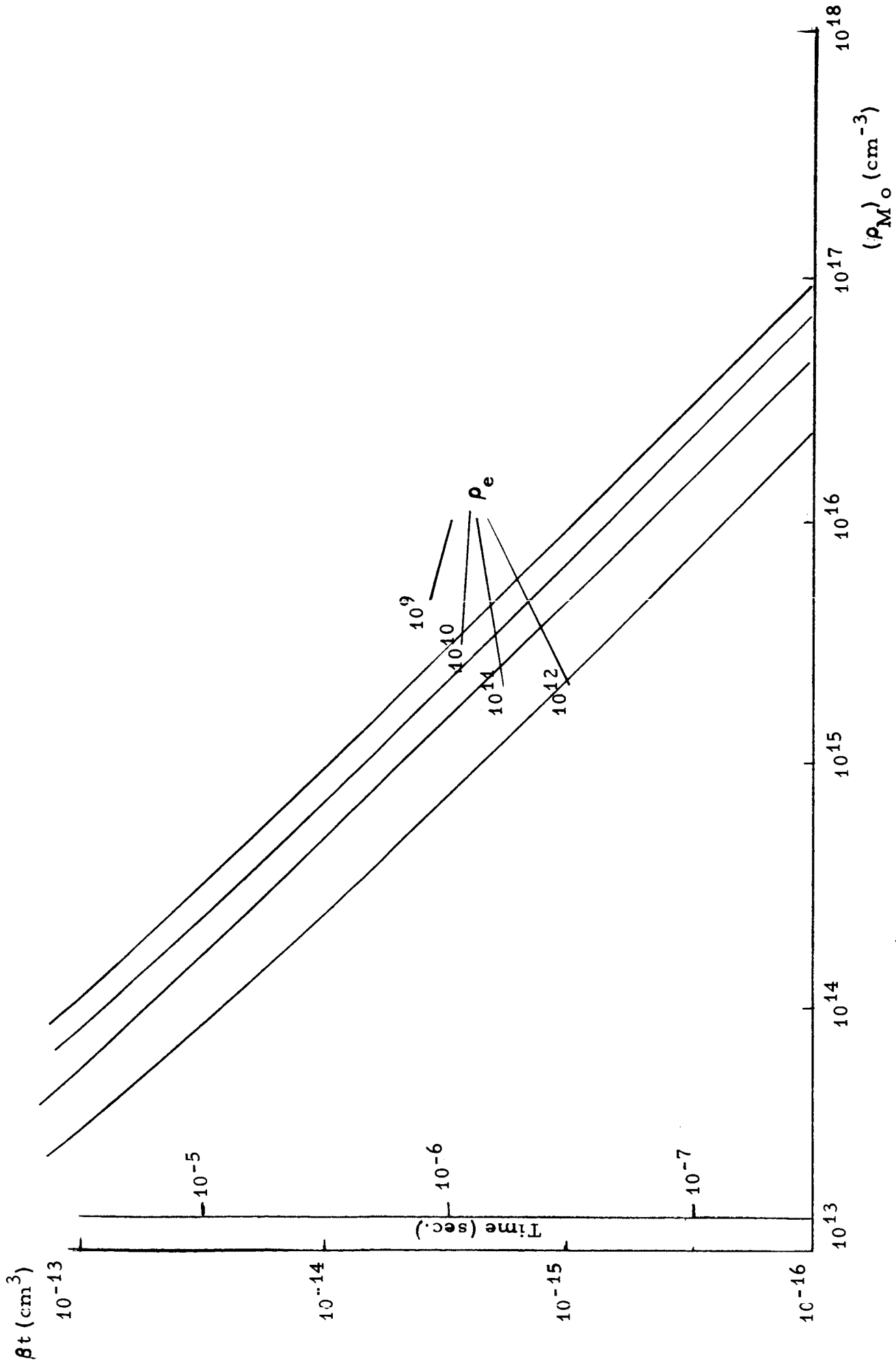
INAZZ

FRANKLIN BNO CORPORATION



$\beta t$  vs  $\rho_e$  FOR VARIOUS VALUES OF  $(\rho_{M_0})_0$

Figure 32



$\beta t$  vs  $(\rho_M)_0$  FOR SPECIFIC VALUES OF  $\rho_e$



SECTION VSUMMARY & CONCLUSIONS

1. An improved technique for measuring both the mobilities and the attachment probabilities of negative ions of mixtures of electrophilic materials with air has been developed. The instrument, though similar in some respects to that used by previous investigators, measures the experimental parameters to an accuracy of better than 10%. This is accomplished by reducing the electric field between the photocathode and control grid to zero during the time that the photopulse is operative.
2. Electron attachment measurements were made in a variety of electrophilic materials at room temperature. The materials include perfluorohexane, perfluoroheptane, perfluorooctane,  $C_8F_{16}O$ , Freon E-3, Freon E-4, and Freon E-5. For most of the materials,  $Q/Q_0$  remained essentially constant, and assumed the value of approximately unity.
3. In some of the perfluorocarbon materials, multiple ion peaks were observed. While it is possible that impurities in the samples caused this unusual behavior, this is highly doubtful. It is much more likely that the samples are mixtures of various isomers, and that electron attachment takes place by both direct capture and by dissociative attachment. This would give rise to the apparent presence of ions of a relatively wide range in mass.
4. One important aspect of the experimental results shown in Table II, is that the value of  $Q/Q_0$  appears to be independent of the concentration of the electrophilic material in the atmosphere, and is near unity. This observation is as expected, and indicates that the equipment is operating properly.
5. A highly simplified calculation of an equilibrium condition for quenching has been made. Although the conditions specified are for room temperature data, the results should be of value for estimating usefulness of the above materials in re-entry situations.
6. Thermal decomposition was observed to start at about 700 - 800° K for three perfluorocarbons:  $C_7F_{16}$ ,  $C_8F_{18}$ , and  $C_8F_{16}O$ . The decomposition was apparently accomplished in two steps, one within a short time of less than a minute, probably established by gaseous equilibrium, the other over a period of 5 - 20 minutes, probably indicating changes in surface conditions of the test cell.

7. Daughter compounds resulting from thermal decomposition retained electrophilic capability which was always greater than for  $\text{SF}_6$  up to  $800^\circ\text{K}$ . It may be possible to realize greater collective electrophilic action from daughter compounds than from the parent, but this was not observed experimentally over the temperature range investigated.

8. High voltage breakdown data was also obtained for  $\text{SF}_6$  (99.99%) up to  $900^\circ\text{K}$ , where considerable decomposition starts to appear.

9. High voltage breakdown constants were obtained for the room temperature relation  $V_s = k_1 P\delta + k_2$ ,  $k_1 = 117, 308, 354, 335$  volts/Torr cm,  $k_2 = 600, 550, 650, 600$  volts, for  $\text{SF}_6$ ,  $\text{C}_7\text{F}_{16}$ ,  $\text{C}_8\text{F}_{18}$ , and  $\text{C}_8\text{F}_{16}\text{O}$  respectively. These constants agree with previously published data.

10. Using the relation that  $\eta/P$  at breakdown is proportional to  $E/P = k_1$  then relative to  $\text{SF}_6$  ( $\eta/P = 1.06$ ,  $k_1 = 117$ , at room temperature) approximate values of  $\eta/P$  for  $\text{C}_7\text{F}_{16}$ ,  $\text{C}_8\text{F}_{18}$ , and  $\text{C}_8\text{F}_{16}\text{O}$  are 2.8, 3.2, and 3.0 respectively. Apparently these values do not change up to  $900^\circ\text{K}$ , and the error in this approximation is large. However, the estimate is obtained with pure samples and not subject to error arising from dilution procedures.

## REFERENCES

1. K. B. MacAfee Jr., J. Chem. Phys., 23, 1435 (1955).
2. W. M. Hickam and R. E. Fox, J. Chem Phys., 25, 642 (1956).
3. L. M. Chanin, A. V. Phelps, and M. A. Biondi, Phys. Rev., 128, 219 (1962).
4. D. Edelson, J. E. Griffiths, and K. B. MacAfee, Jr., J. Chem. Phys., 37, 917 (1962).
5. E. W. McDaniel, "Collision Phenomena in Ionized Gases," John Wiley & Sons, N. Y. (1964), P. 492.
6. E. W. McDaniel, Ibid, Chapter 8.
7. J. S. Townsend, Electricity in Gases, Clarendon Press, Oxford (1915).
8. R. Geballe and M. L. Reeves, Phys. Rev., 92, 867 (1953).
9. H. Raether, "Electron Avalanches and Breakdown in Gases," Butterworths (Washington), 1964.
10. R. W. Crowe, Unpublished Data.
11. R. E. Banks, "Fluorocarbons and Their Derivatives," Oldbourne Press, London (1964).
12. R. W. Crowe, J. Appl. Phys., 37, 1515 - 1527 (1966).